LHCb-PUB-2017-020

Performance of the RASNIK Optical Alignment Monitoring System for the LHCb Outer Tracker Detector

Marek Szczekowski[1], Niels Tuning[2], Artur Ukleja[1], Robert Hart[2], Antonio Pellegrino[2], Krzysztof Syryczyński[1].

[1] *National Centre for Nuclear Physics, Warsaw, Poland*
[2] *Nikhef National Institute for Subatomic Physics, Amsterdam, Netherlands*

LHCb-PUB-2017-020
24/10/2017

Abstract

We present the results collected by an optical system for position control of the Outer Tracker detector stations in the LHCb experiment. This system has been constructed using the RASNIK three-point alignment monitors. The measurements are based on data taken in Run 2 of LHC.

Contents

1 Introduction

The construction of very large detectors for Large Hadron Collider (LHC) at CERN, as for instance the LHCb detector [1], requires often a precise alignment of their elements. In this paper we present the results from the system of precision sensors built to periodically monitor position of the Outer Tracker (OT) - the main tracking detector in the LHCb experiment, to improve the performance and provide the control of the detector. This system was constructed using the **R**elative **A**lignment **S**ystem of **NIK**HEF (RASNIK). The description of the system for the OT is presented in Sec. 2. The results obtained using data taken during running of LHC Run 2 are shown in Sec. 3 for 48 short horizontal lines and in Sec. 4 for two long vertical lines of the RASNIK system. In Sec. **??** the RASNIK measurements are compared to results of the BCAM position system for the Inner Tracker (IT) detector. Conclusions are presented in Sec. 5.

The data discussed in this note are taken in the period from 27 April 2016 till 30 November 2016. They consist of a part of Run 2 of LHC.

2 The RASNIK system

The idea of the RASNIK system [2–5] is to project a finely detailed image of a coded mask through a lens onto a CCD camera (Fig. 1). If any of these three elements moves, there will be a corresponding movement of the image on the CCD camera.

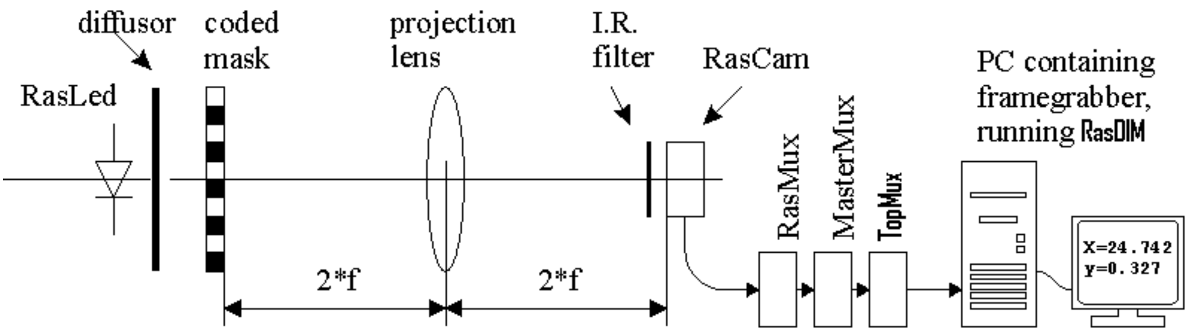

Figure 1: The scheme of the RASNIK alignment monitoring system. The image of a coded mask is projected through a lens on a CCD camera and then transmitted as a standard video signal to a computer through a chain of multiplexers.

The light source is a 3 × 3 grid of infrared-emitting LEDs. These LEDs illuminate a coded mask. The mask consists of black-and-white squares in almost a checker-board pattern (Fig. 2). Since only a small section of the mask is seen by the CCD camera, the coded non-repeating pattern is used to obtain a unique position. The image is focussed with a simple convex lens placed near or at half-way point between the mask and the camera. Since the movement of the lens by a distance d in a direction perpendicular to the axis defined by the mask and the CCD camera causes displacement of the image of the mask by a distance 2d (Fig. 2), the change of a transverse position of the lens is calculated from the image position by means of image processing of a CCD pixel frame. The image on the CCD is transmitted as a standard video signal to a computer where a single frame is digitised and recorded as a binary file. From these data the RASNIK software first finds positions of black and white transitions of the image recorded by the CCD camera and then reconstructs positions of the lines on a chessboard. Finally, coordinates perpendicular to the optical axis – X and Y, scale (magnification) and rotation angle around optical axis – α are calculated. The scale is calculated from a size of the image. Planes of the camera and the mask are parallel to each other, thus two scales in directions X and Y are the same. The system uses only one scale – size of the image in the Y direction. From the scale a change of the coordinate Z of the mask is calculated.

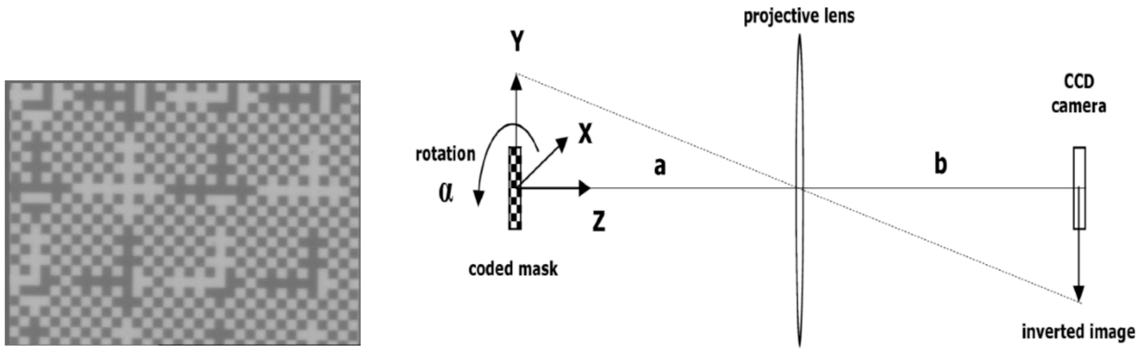

Figure 2: A part of the mask as seen by a camera (left) and a local X, Y, Z coordinate system for a RASNIK line (right).

The resolution of the CCD-RASNIK system in terms of lens displacement perpendicular to the optical axis is better than 1 μm for a system with a mask-to-CCD distance up to about 8 m [2]. Movements along the axis are measured though the change in the size of the image. The resolution in the longitudinal direction is usually better than 150 μm. In this paper we will show results only for more precise measurements of displacements perpendicular to the optical axis. The maximum transverse measurement range of the system is limited only by a diameter of the mask.

Since RASNIK does not provide information about which of the three elements moved, to reduce ambiguity in the system for the LHCb OT detector, two RASNIK elements are mounted on a rigid shelf. The position of the third element with respect to the position of the shelf is measured.

The modules of straw drift tubes of the LHCb OT are mounted on 12 frames of a C-shape, about 3 m long and 5 m high, made of aluminium. The C-frames move on rails fixed under the stainless steel bridge supported by two pillars standing on the concrete bunker (Fig. 3).

The elements of 48 RASNIK lines are mounted on the four corners of each of the 12 C-frames. They measure displacements of four points on a C-frame in respect to corresponding reference points – shelves with other RASNIK elements mounted on the bridge, the pillars and on a special table fixed to the bunker (Fig. 4).

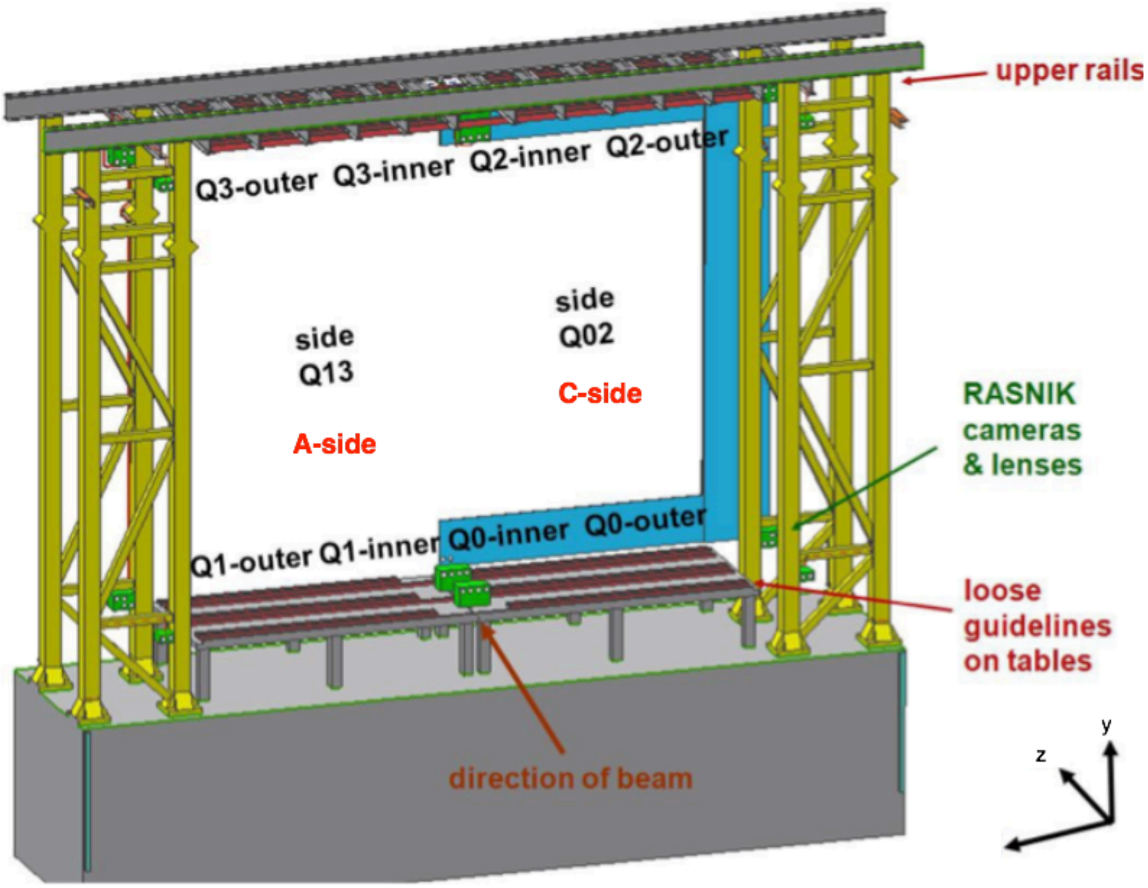

Figure 3: A general view of a part of the Outer Tracker detector showing the supporting bridge with some elements of 48 horizontal RASNIK lines mounted on shelves fixed to the bridge, on the pillars and on the tables. The A-side and C-side are defined in the figure.

All RASNIK masks are fixed to moveable C-frames (Fig. 5) and all CCD cameras are mounted on the stable shelves (Figs 6 and 7). To reduce ambiguity of the movements of three RASNIK elements lens is fixed together with either a CCD camera or with a mask on the same rigid support. Most lenses are fixed together with cameras on rigid shelves. Only lines in the middle positions for the OT station T1 have lenses mounted on C-frames together with masks due to lack of space close to the magnet.

In addition to 48 short horizontal lines measuring mainly x and y LHCb coordinates of C-frames positions with respect to the bridge and tables, there are two long vertical lines (Fig. 8) measuring horizontal x and z LHCb coordinates of the two top points on the bridge with respect to the bunker with high precision.

The 48 RASNIK monitor lines are read-out in sequence by multiplexers (RasMuX). The RasMuX is a video and pixelclock multiplexer and controller for cameras and LED of the RASNIK system. It is placed in the bunker. In the present version RasMuX has I/0 for 12 LEDs and 8 cameras.

The RasMuX is controlled from a special unit (MasterMuX) with JTAG control signals. At this level the JTAG control signals are LVDS. Also the power for the RasMuX is provided via its MasterMux cable. The RasMux selects LED and camera lines for operation under JTAG control by switching on the appropriate power lines and multiplexing the

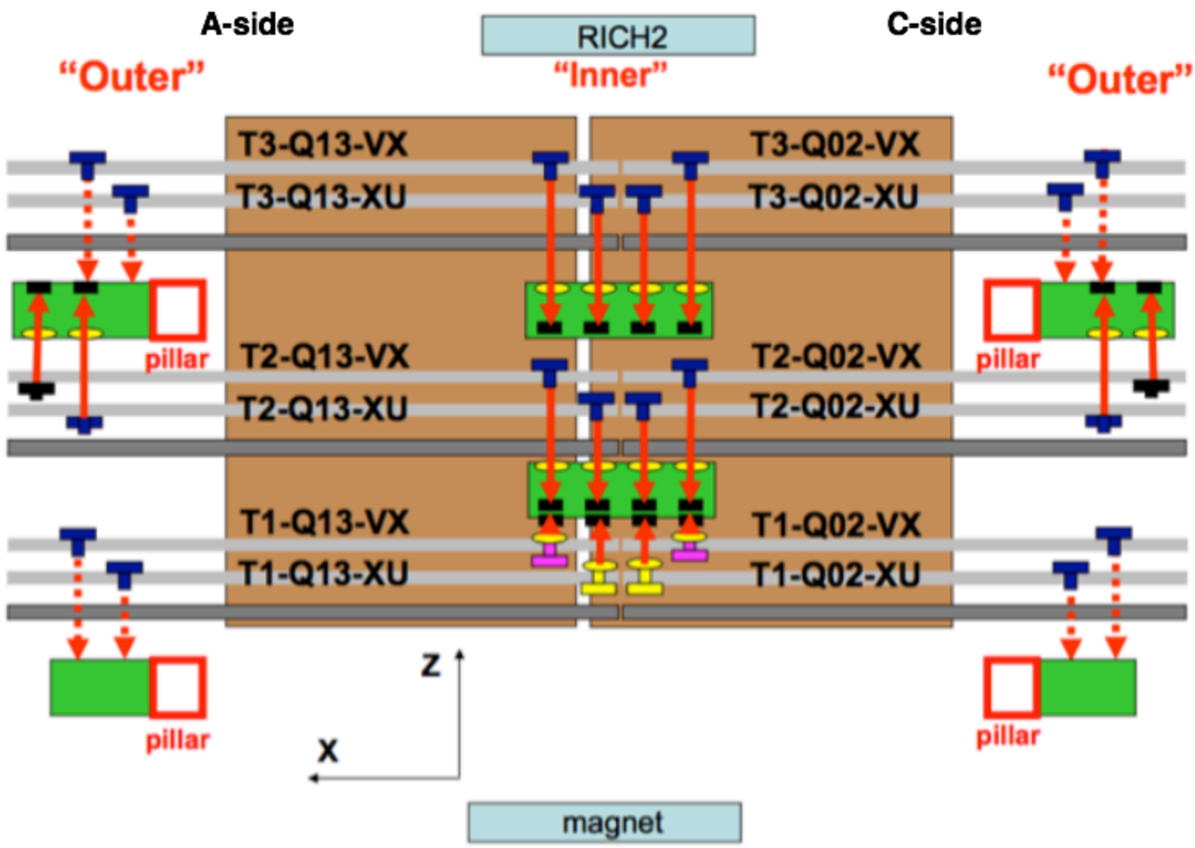

Figure 4: A schematic top view of 24 horizontal RASNIK lines for the lower corners of C-frames. Six pairs of C-frames (light grey) and three planes of the Inner Tracker detector (dark grey) are grouped together in the three stations of the main tracking detector of the LHCb experiment. The labels for 12 C-frames of the Outer Tracker are shown. The dotted lines show RASNIK lines with elements mounted below a shelf (see Fig. 6). A similar scheme can be drawn for the 24 lines in the upper corners of C-frames.

Figure 5: Two sides of a RASNIK mask mounted on a C-frame.

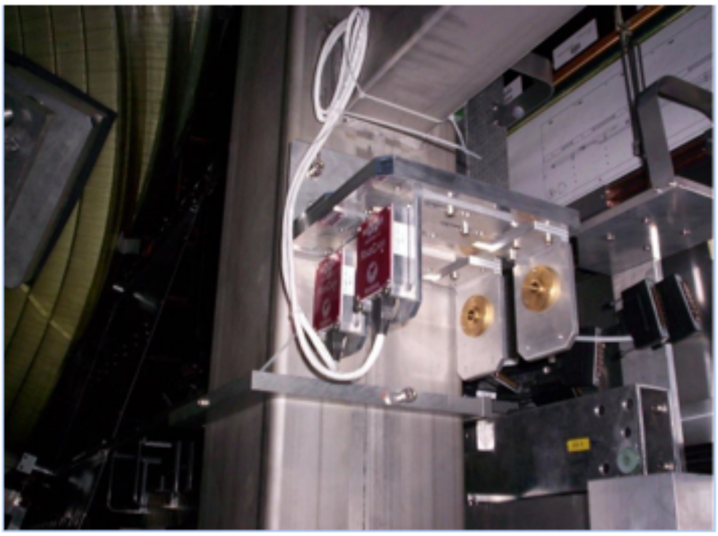

Figure 6: A RASNIK shelf mounted on a pillar with lenses and cameras of two lines monitoring frames in T1 station of the Outer Tracker detector.

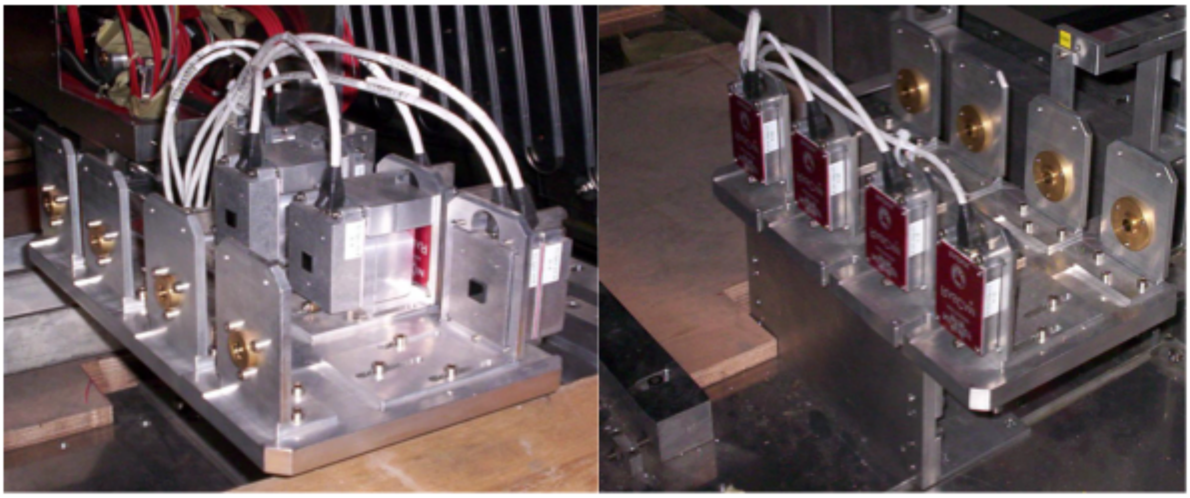

Figure 7: Two RASNIK shelves mounted on the table with lenses and cameras of four inner lower RASNIK lines monitoring T1 and T2 (left) and T3 (right) stations of the Outer Tracker detector.

incoming camera video and pixelclock signals to the MasterMux. Power switching of the cameras (+12V) and LEDs (+24V) is done with industrial short-circuitproof power devices.

The video standard used is CCIR. The RASNIK prototype system with the analysis and JTAG software is PC based and uses PCI Video Digitizer (Frame Grabber DT 3152 from Data Translation). It performs a pixelsynchronous digitisation and reduces the video frame to pixel (384 x 287) data, producing an output file of 128 kB.

The read-out and analysis of one sequence of 50 RASNIK lines takes about 2 min. of PC (130 MHz).

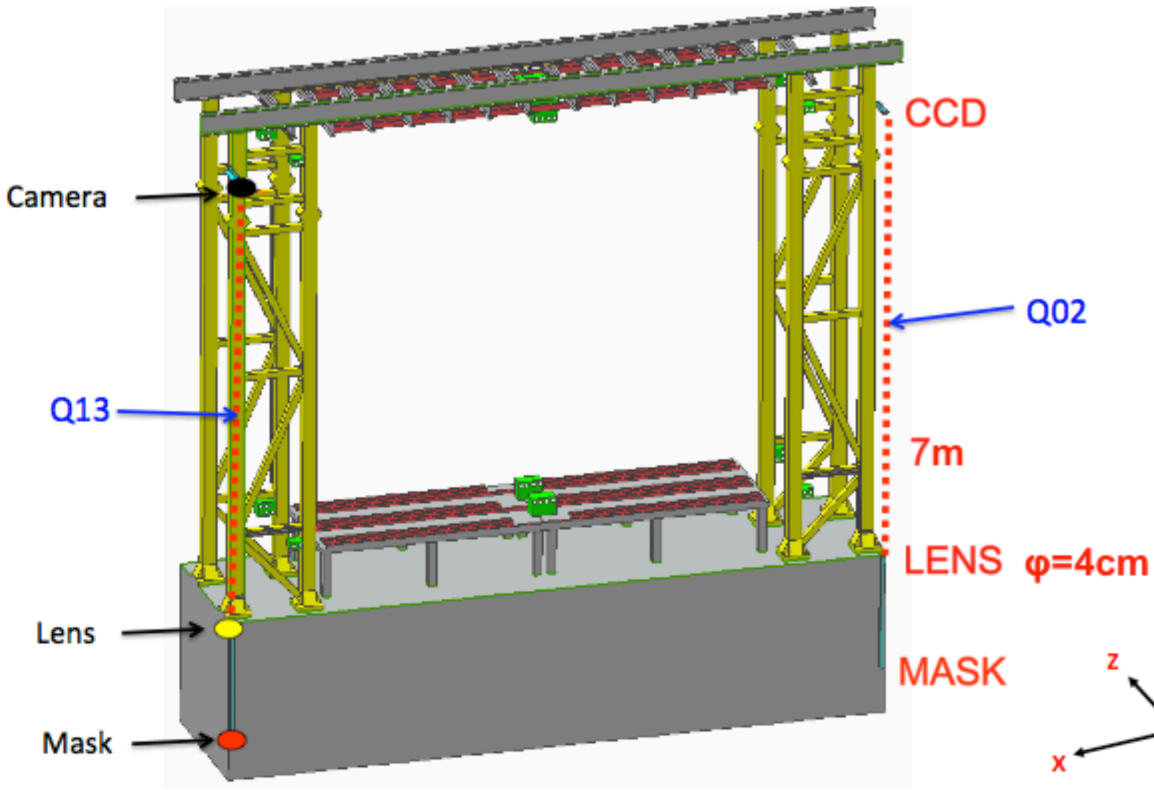

Figure 8: Two long vertical RASNIK lines (Q13 and Q02) mounted on the bridge (a CCD camera) and the bunker (a lens and a mask) to measure the movements of two points close to the top of the bridge in horizontal x and z LHCb coordinates with high precision.

Figure 9: A CCD camera of a long vertical RASNIK line mounted on the bridge (left). A lens and a mask fixed together to the bunker's wall (right).

3 Monitoring of C-frames positions by 48 RASNIK horizontal lines

3.1 Long term stability of C-frames positions

The 48 horizontal RASNIK lines (Fig. 4) measure the movements of C-frames with respect to the pillars or the tables. They measure the horizontal x and vertical y variations of positions of the points close to the corners of the frames. The changes in the x and y are shown in Figs 10-15 and Figs 16-21, respectively.

In general, the RASNIK results show the following features:

- the top parts of the C-frames are more stable ~ 50 μm in time than the bottom ones ~ 200 μm, in both x and y coordinates. It is consistent with the construction of the C-frames, which are fixed to the bridge on the top and they are hanging at the bottom loosely constrained in z by the rails.
- The positions of the bottom of the C-frames vary within ~ 200 μm in both x and y in 2016. At the beginning, in May and June the changes are relatively large ($100 - 200$ μm), they stabilize in August but in September they start to evolve with the opposite trend with respect to the early period.
- There are also sudden position changes visible either as short "jumps" or as steps in the distributions. The "jumps" are caused by the power cuts. The steps correspond to the periods when the magnet was switched off.

All above effects are discussed in details in the following parts of this note.

Results from some lines are not available due to mechanical conflicts in the construction of the caterpillar track of the IT. These lines are mounted on the external corners on the bottom parts of C-frames of OT stations. For the VX C-frame of the T3 station the line mounted on the bottom internal corner is not working as well.

Since the positions changes of C-frame in x and y are observed in time in Figs 10-21, it is interesting to check the correlated movements in the x and y planes. These variations are shown in Figs 22 and 23 for data acquired in 27 April – 20 June 2016 and in Figs 24 and 25 for data acquired in 16 September – 10 October 2016. The movements in y are correlated with the movements in x and the magnitudes of these changes are similar in both coordinates. Some C-frames move, however, in a more complicated way suggesting the rotation of the frames.

To summarize, the movements of the C-frames in the x and y coordinates are relatively large (up to 200 μm) within the first month of data taking and stabilize to $30 - 50$ μm in the following periods. The correlations between the x and y are observed and show that the movements are more complicated than simple shifts in x or y positions. In the next section we show that these movements can be also observed in lengths variations of C-frames.

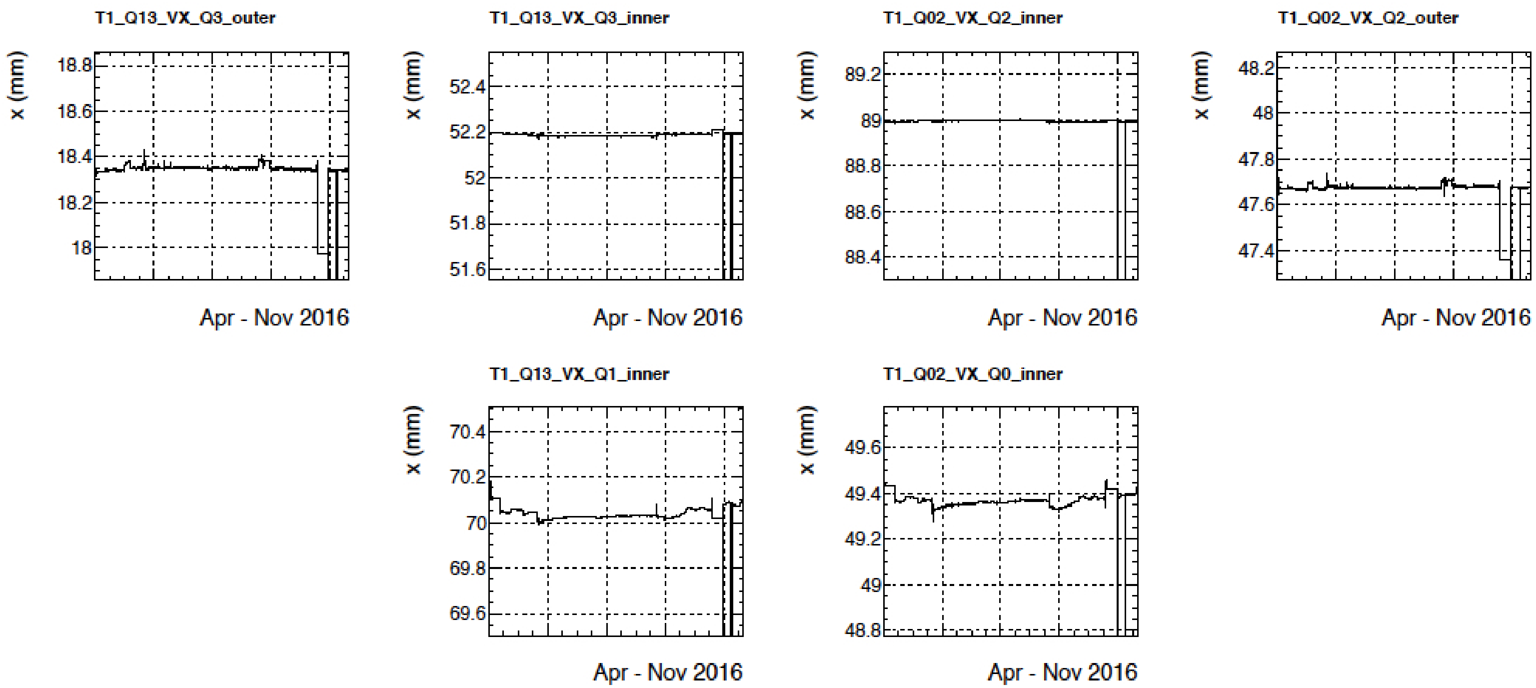

Figure 10: The movements of four corners of **two VX C-frames of T1 station** of the Outer Tracker detector are shown as an x**-coordinate** function of time for the data acquired in 2016. The results from two lines mounted on the external corners on the bottom parts of C-frames are not available.

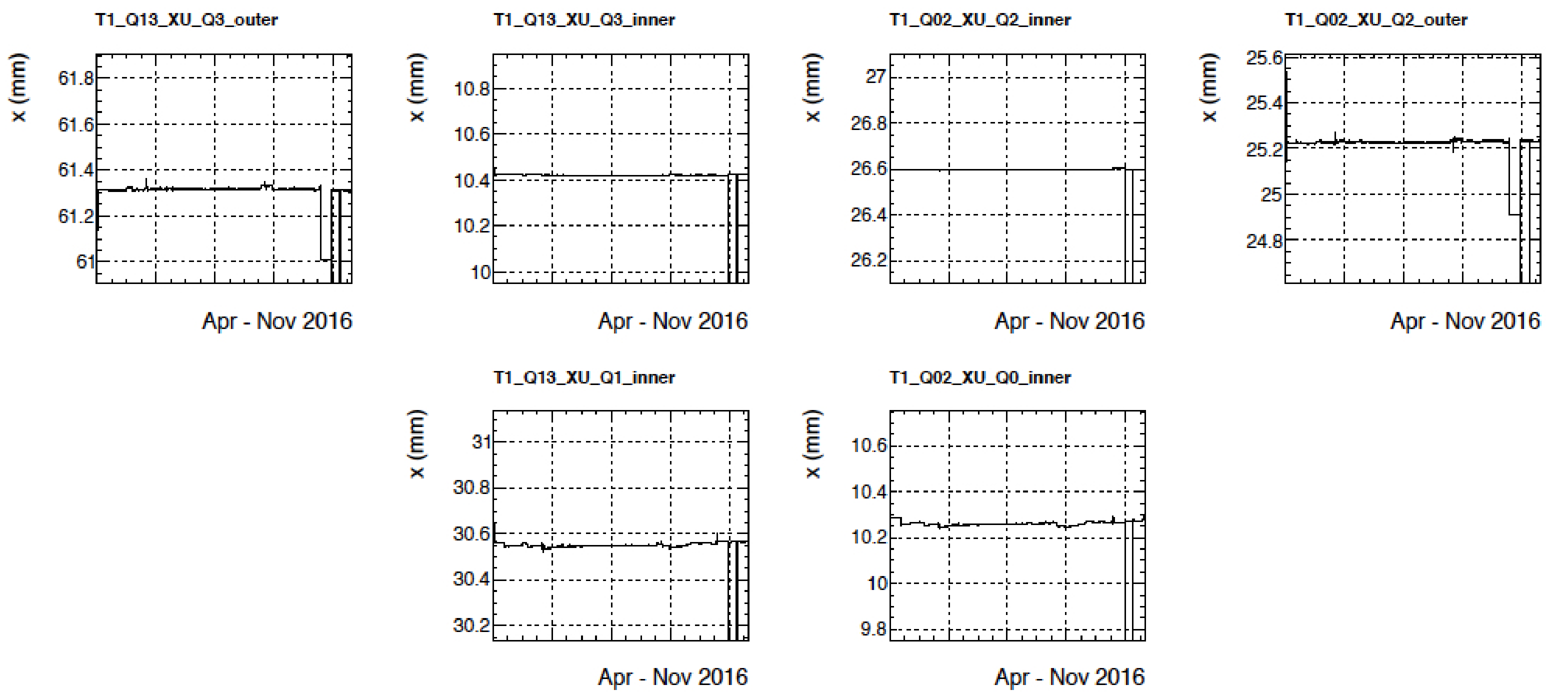

Figure 11: The movements of four corners of **two XU C-frames of T1 station** of the Outer Tracker detector are shown as an x-**coordinate** function of time for the data acquired in 2016. The results from two lines mounted on the external corners on the bottom parts of C-frames are not available.

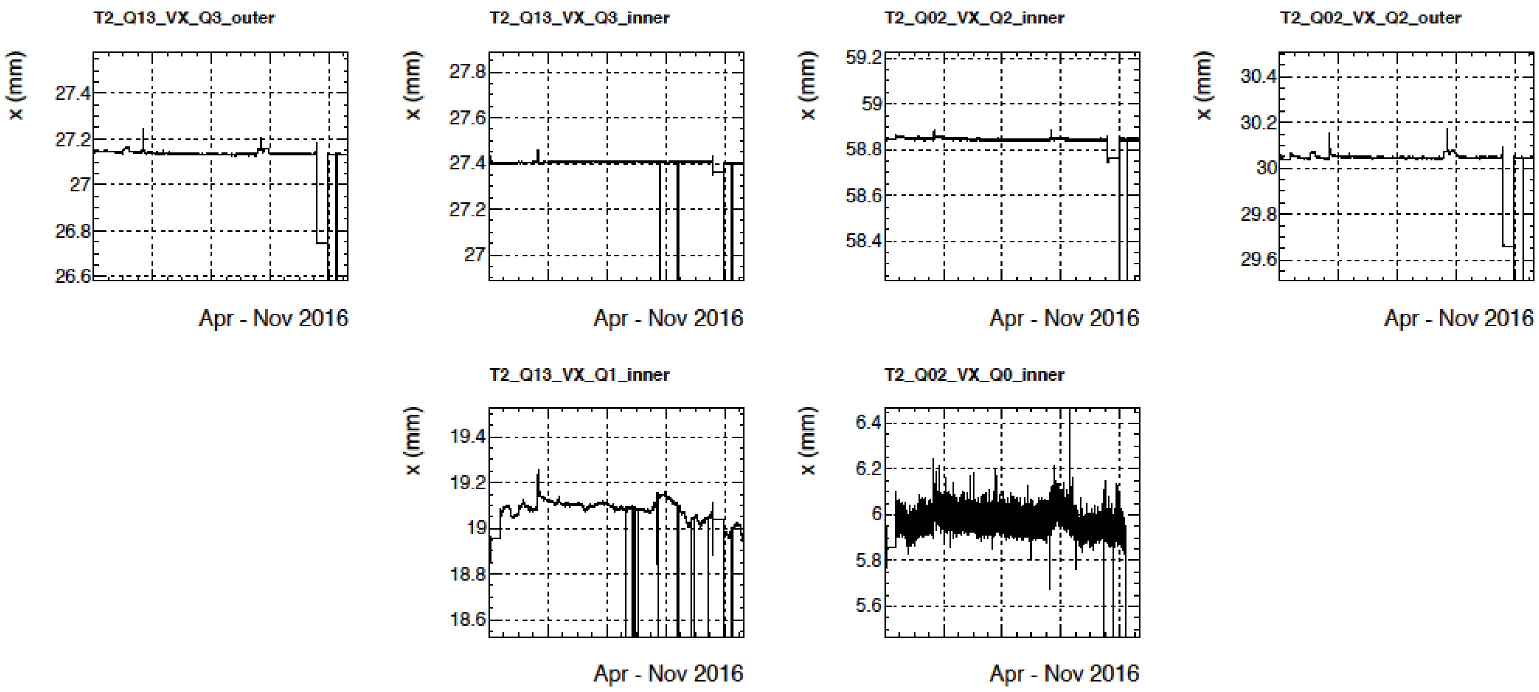

Figure 12: The movements of four corners of **two VX C-frames of T2 station** of the Outer Tracker detector are shown as an x-**coordinate** function of time for the data acquired in 2016. The results from two lines mounted on the external corners on the bottom parts of C-frames are not available.

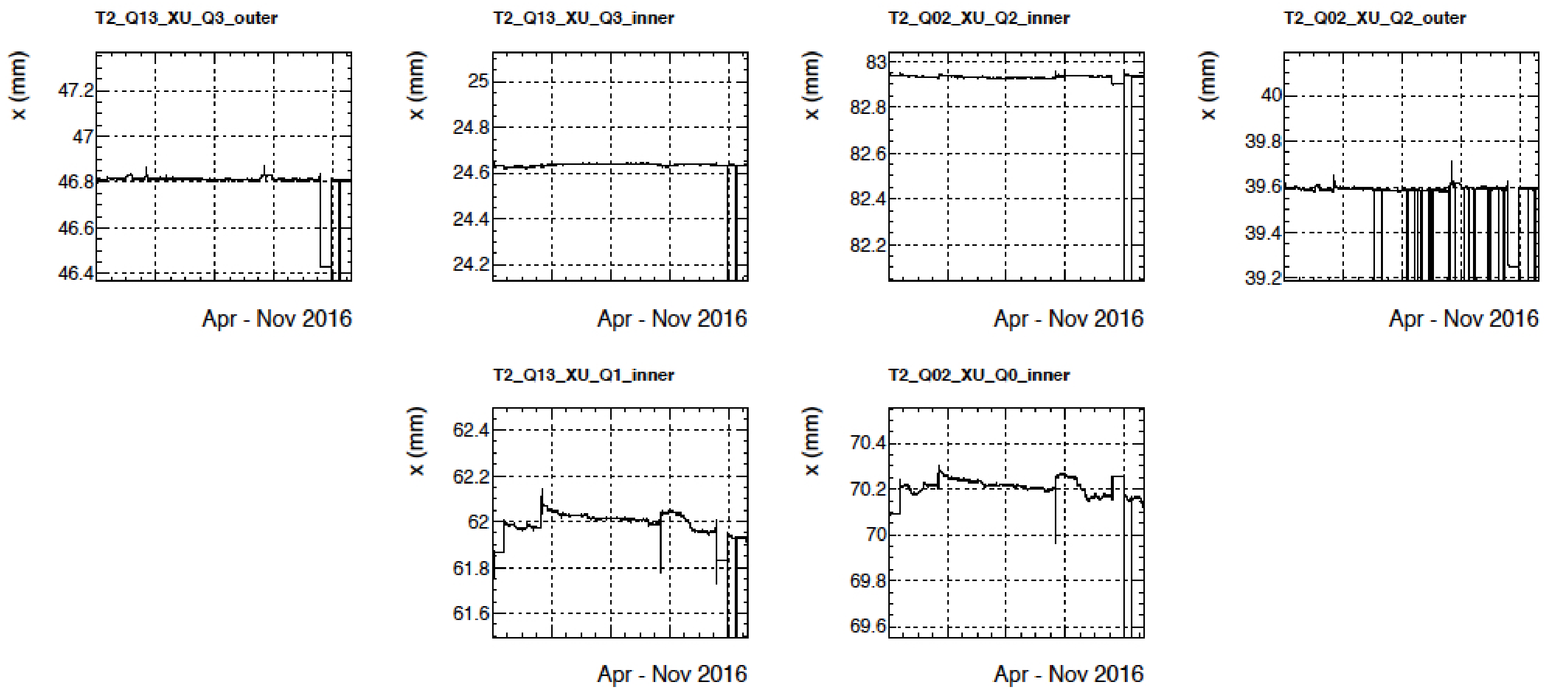

Figure 13: The movements of four corners of **two XU C-frames of T2 station** of the Outer Tracker detector are shown as an x-**coordinate** function of time for the data acquired in 2016. The results from two lines mounted on the external corners on the bottom parts of C-frames are not available.

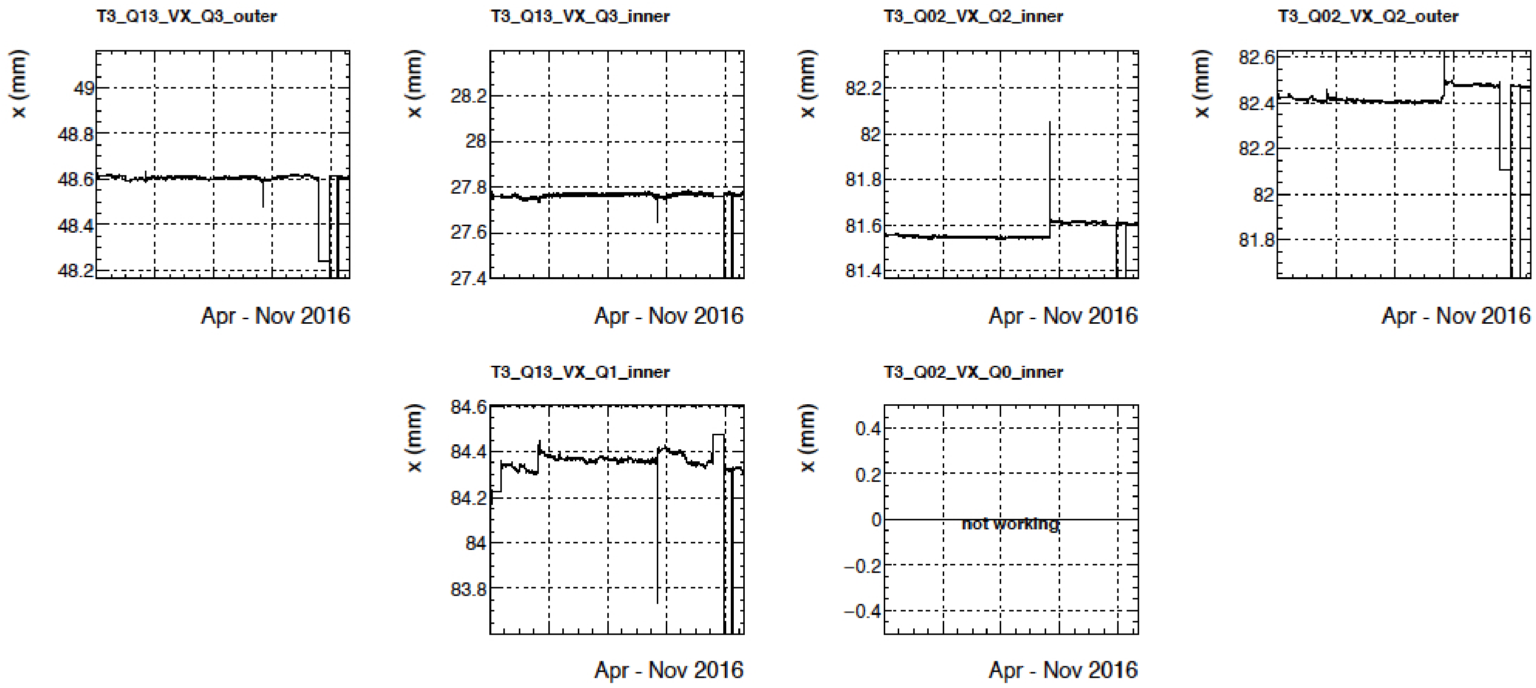

Figure 14: The movements of four corners of **two VX C-frames of T3 station** of the Outer Tracker detector are shown as an x-**coordinate** function of time for the data acquired in 2016. The results from two lines mounted on the external corners on the bottom parts of C-frames are not available.

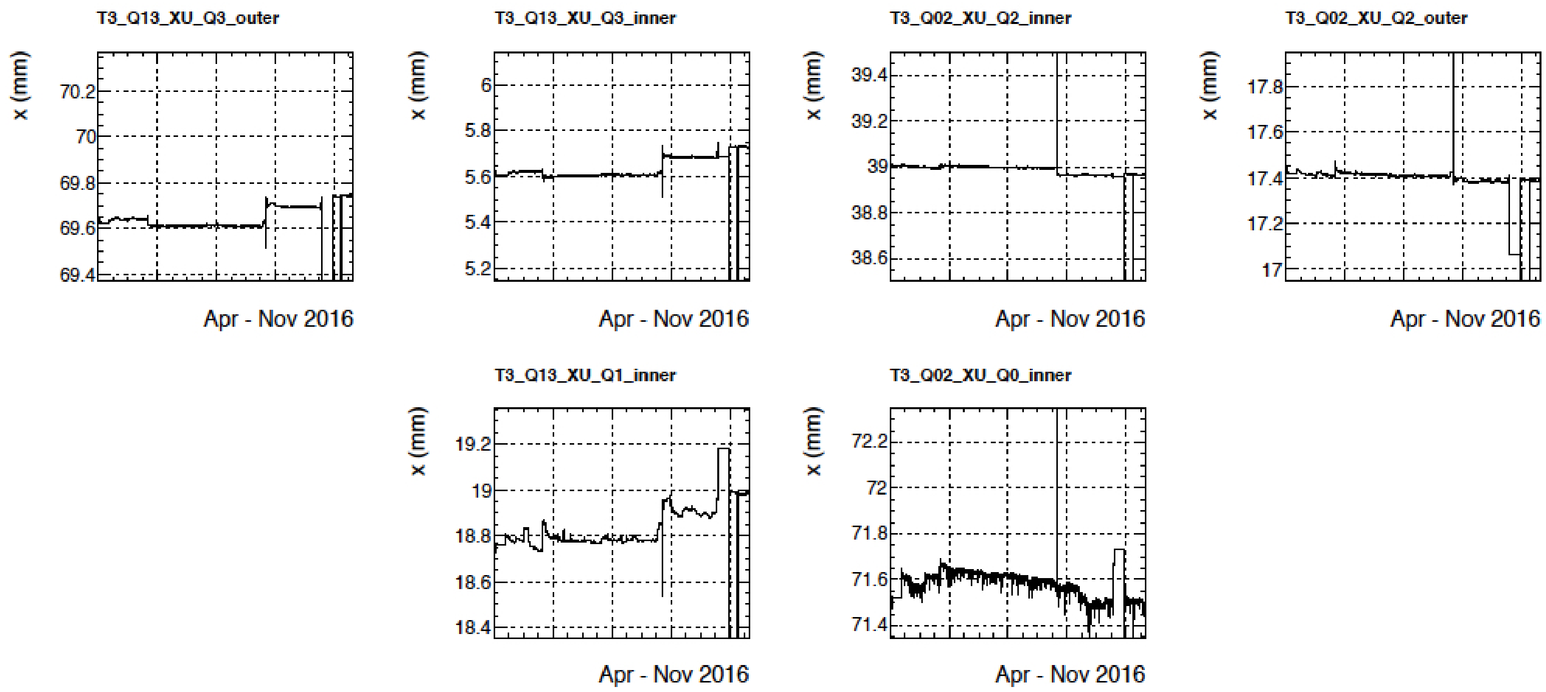

Figure 15: The movements of four corners of **two XU C-frames of T3 station** of the Outer Tracker detector are shown as an x**-coordinate** function of time for the data acquired in 2016. The results from two lines mounted on the external corners on the bottom parts of C-frames are not available.

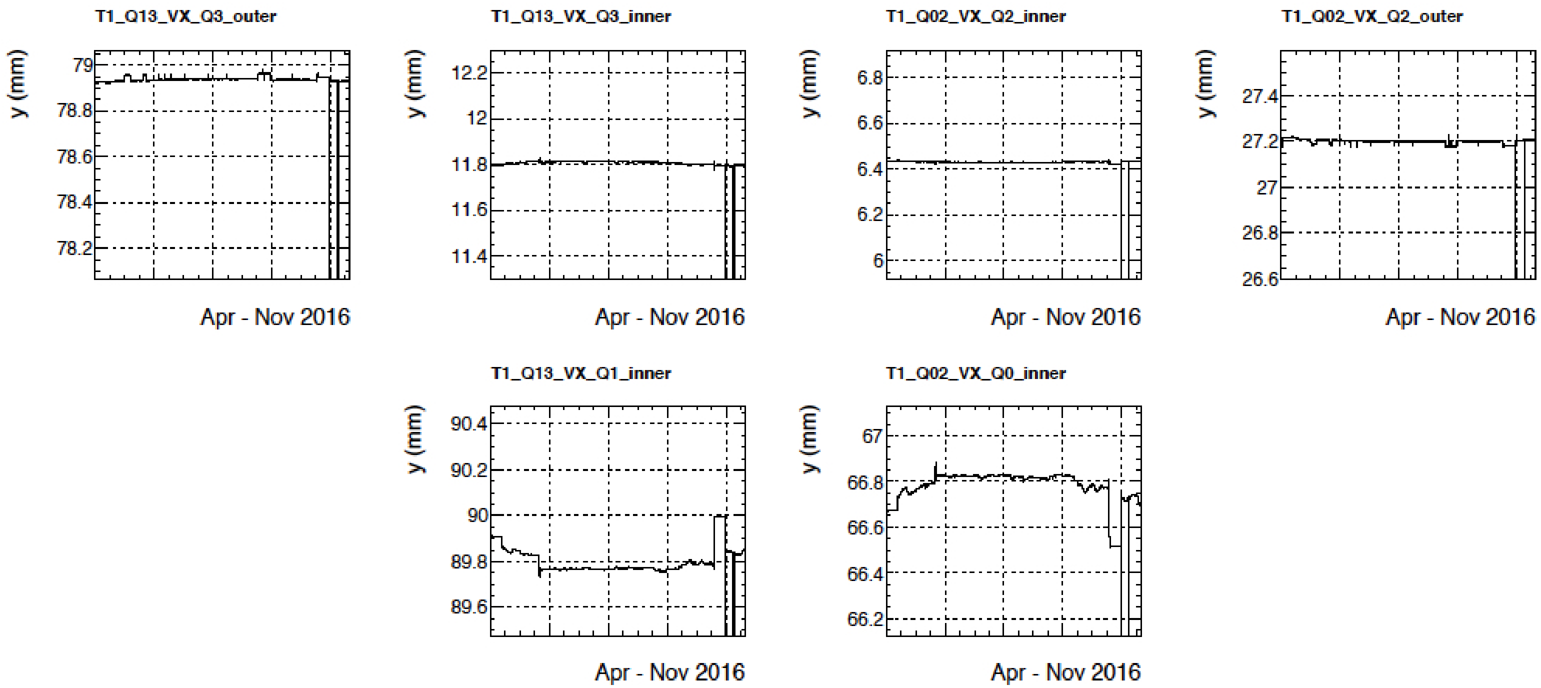

Figure 16: The movements of four corners of **two VX C-frames of T1 station** of the Outer Tracker detector are shown as a y-**coordinate** function of time for the data acquired in 2016. The results from two lines mounted on the external corners on the bottom parts of C-frames are not available.

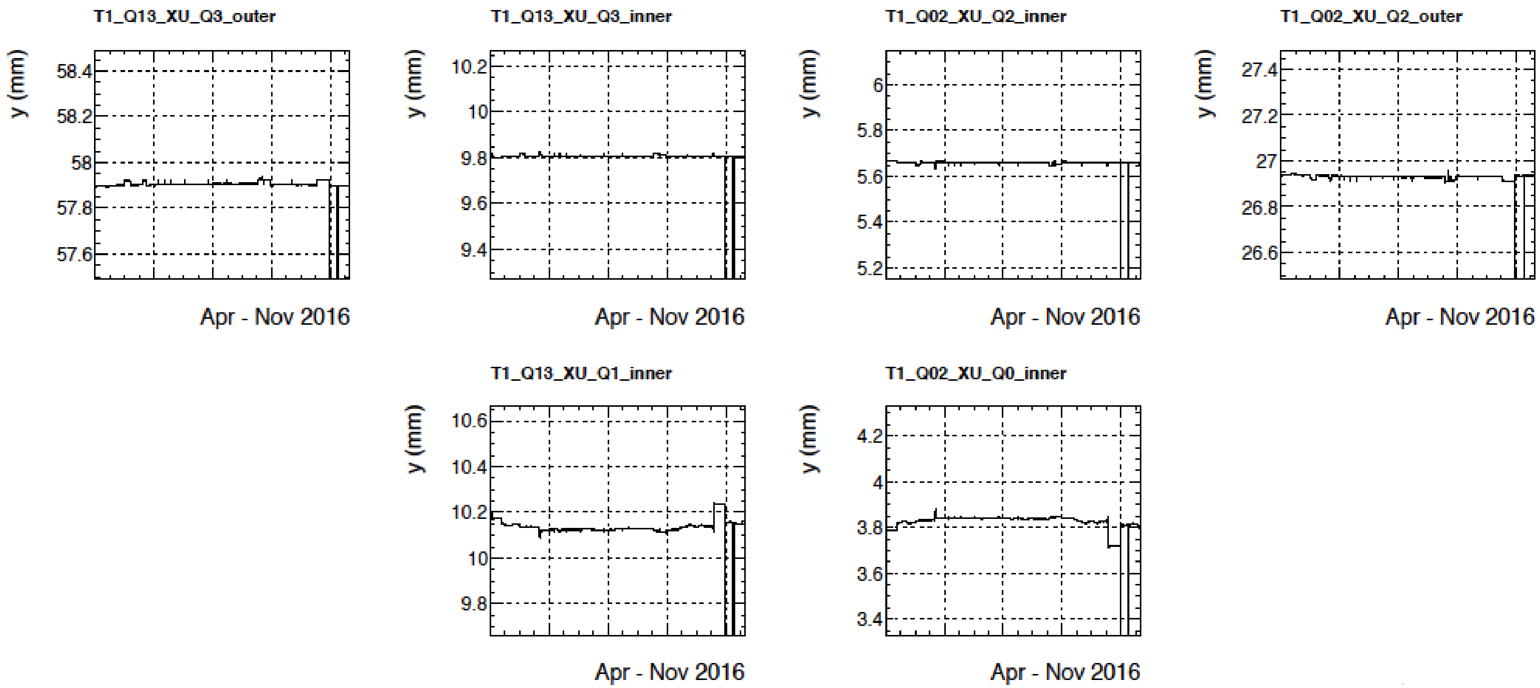

Figure 17: The movements of four corners of **two XU C-frames of T1 station** of the Outer Tracker detector are shown as a y**-coordinate** function of time for the data acquired in 2016. The results from two lines mounted on the external corners on the bottom parts of C-frames are not available.

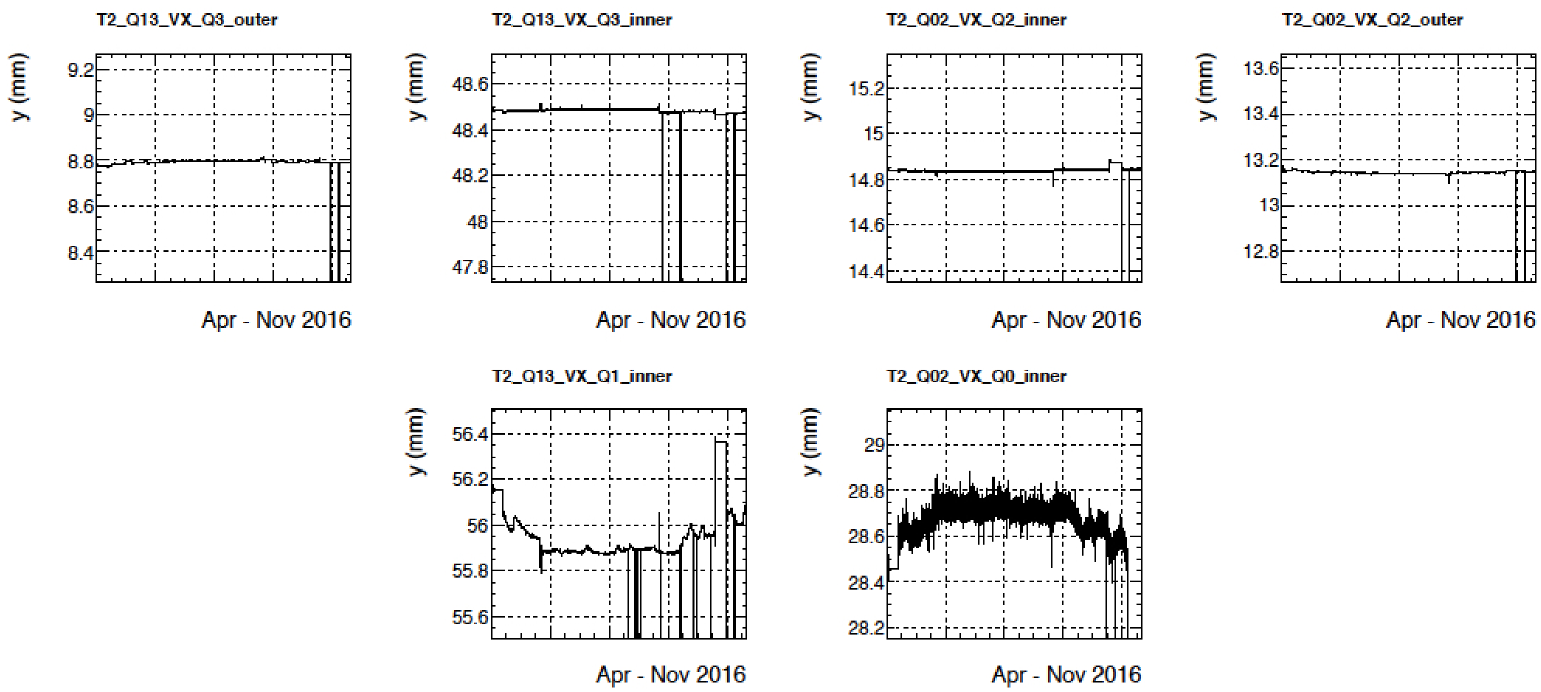

Figure 18: The movements of four corners of **two VX C-frames of T2 station** of the Outer Tracker detector are shown as a y-**coordinate** function of time for the data acquired in 2016. The results from two lines mounted on the external corners on the bottom parts of C-frames are not available.

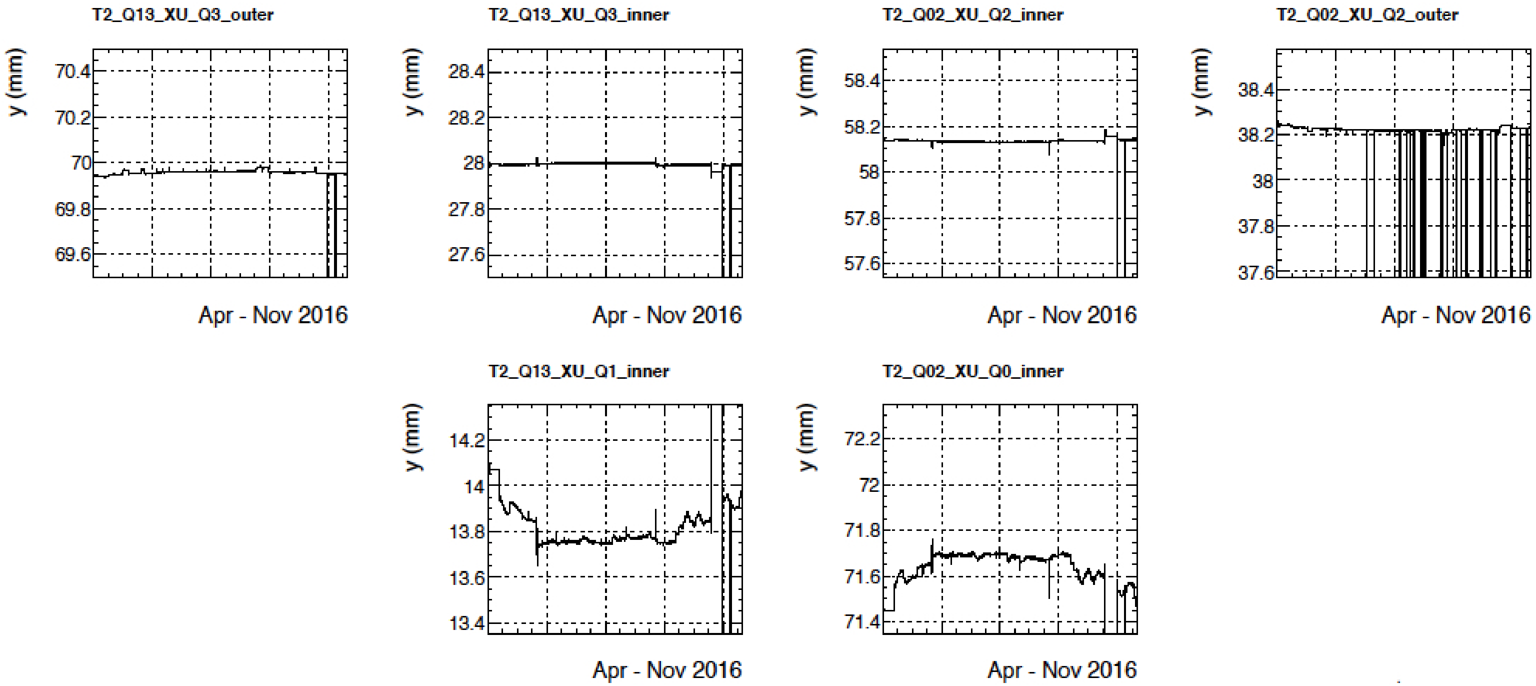

Figure 19: The movements of four corners of **two XU C-frames of T2 station** of the Outer Tracker detector are shown as a y-**coordinate** function of time for the data acquired in 2016. The results from two lines mounted on the external corners on the bottom parts of C-frames are not available.

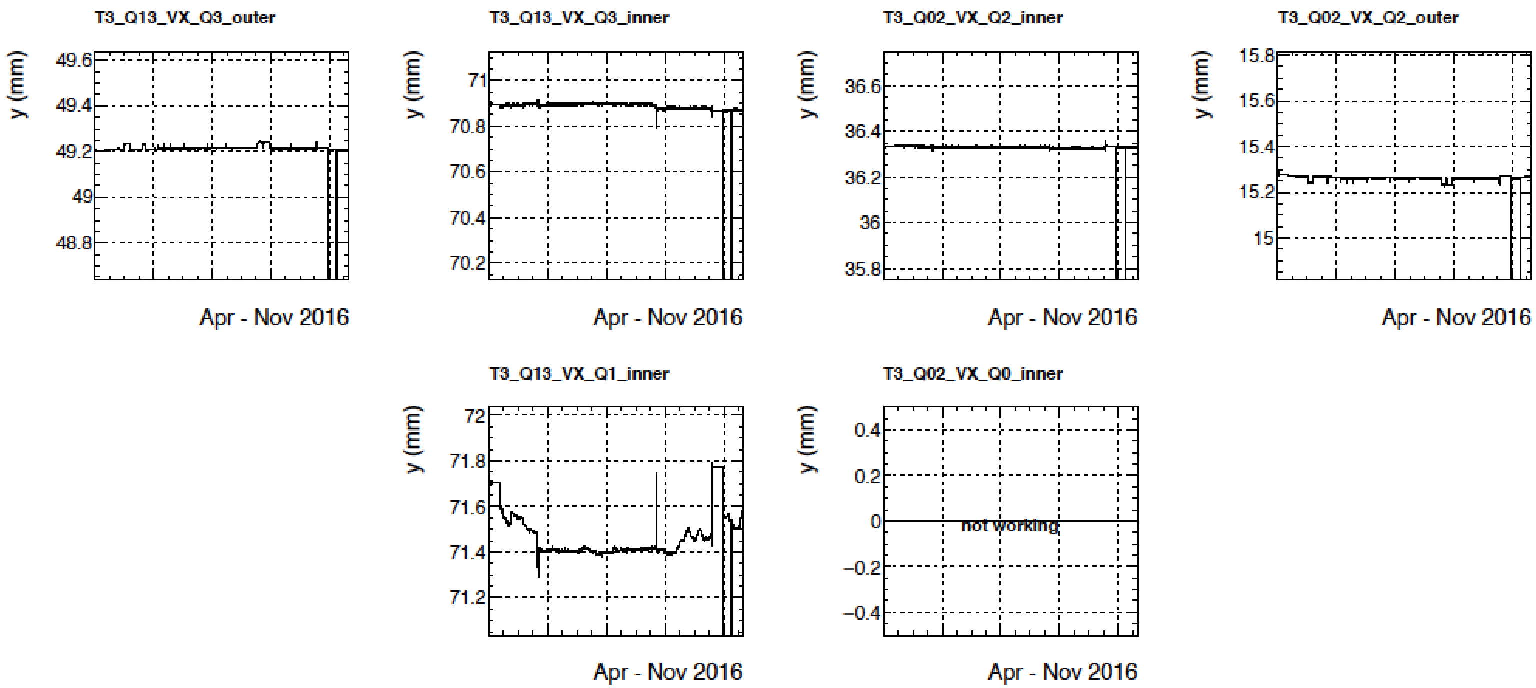

Figure 20: The movements of four corners of **two VX C-frames of T3 station** of the Outer Tracker detector are shown as a y-**coordinate** function of time for the data acquired in 2016. The results from two lines mounted on the external corners on the bottom parts of C-frames are not available.

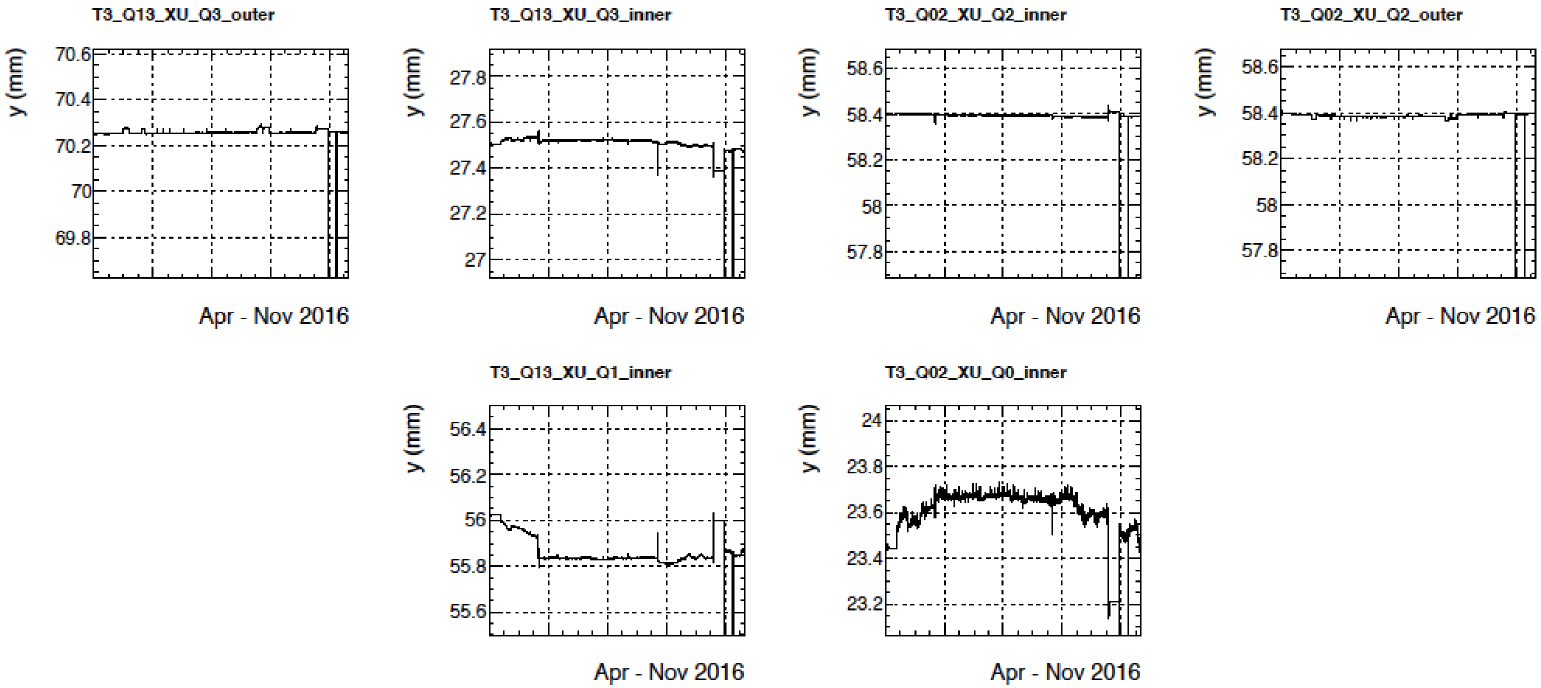

Figure 21: The movements of four corners of **two XU C-frames of T3 station** of the Outer Tracker detector are shown as a y**-coordinate** function of time for the data acquired in 2016. The results from two lines mounted on the external corners on the bottom parts of C-frames are not available.

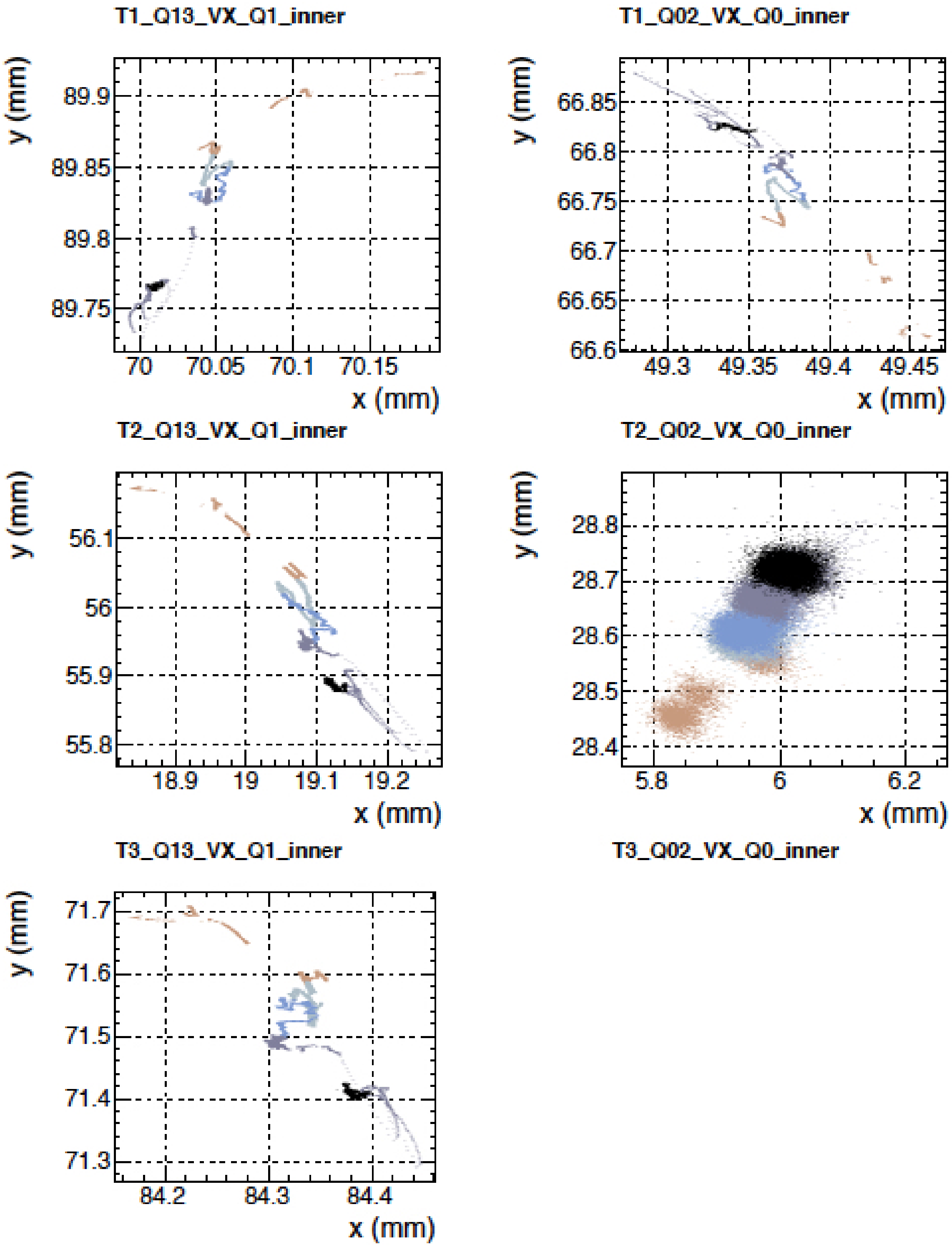

Figure 22: The movements of internal bottom corners of **VX C-frames** in x, y plane in a period of 27 April – 20 June 2016 for T1-T3 stations. The data are divided into five equal periods subsamples from light brown color to dark blue and black, from the first to the last subsample of time, respectively.

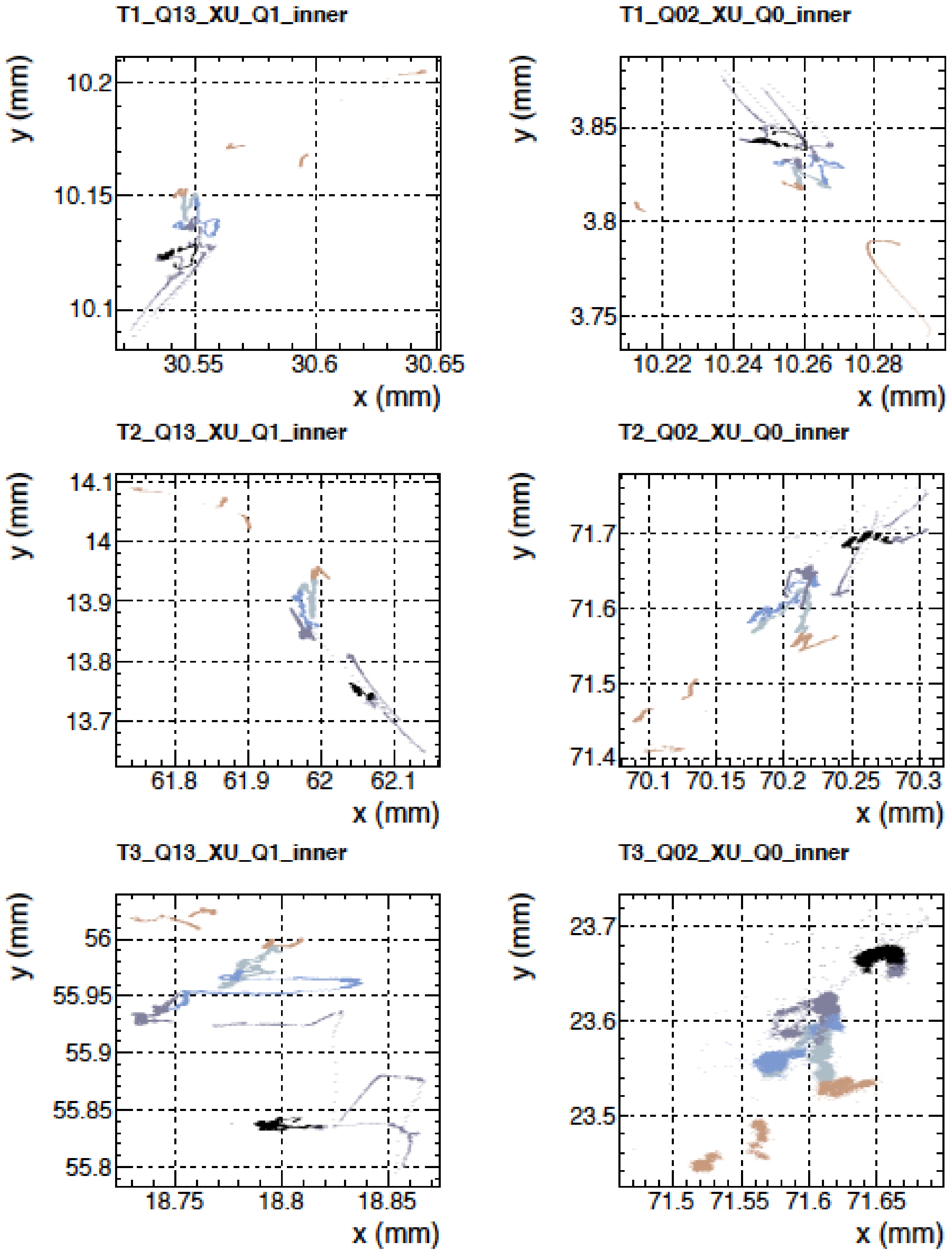

Figure 23: The movement of internal bottom corners of **XU C-frames** in x, y plane in a period of 27 April – 20 June 2016 for T1-T3 stations. The data are divided into five equal periods subsamples from light brown color to dark blue and black, from the first to the last subsample of time, respectively.

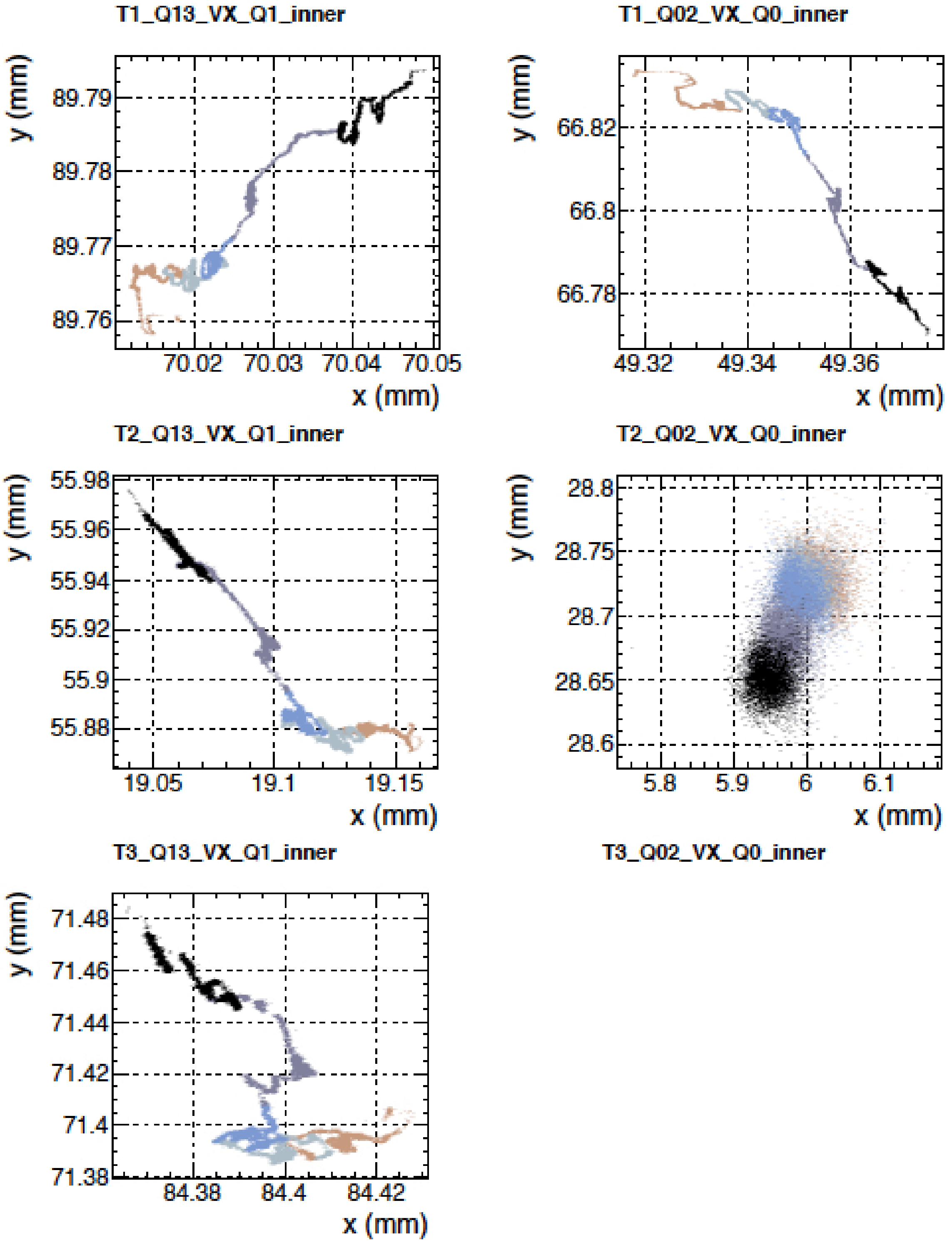

Figure 24: The movement of internal bottom corners of **VX C-frames** in x, y plane in a period of 22 September – 10 October 2016 for T1-T3 stations. The data are divided into five equal periods subsamples from light brown color to dark blue and black, from the first to the last subsample of time, respectively.

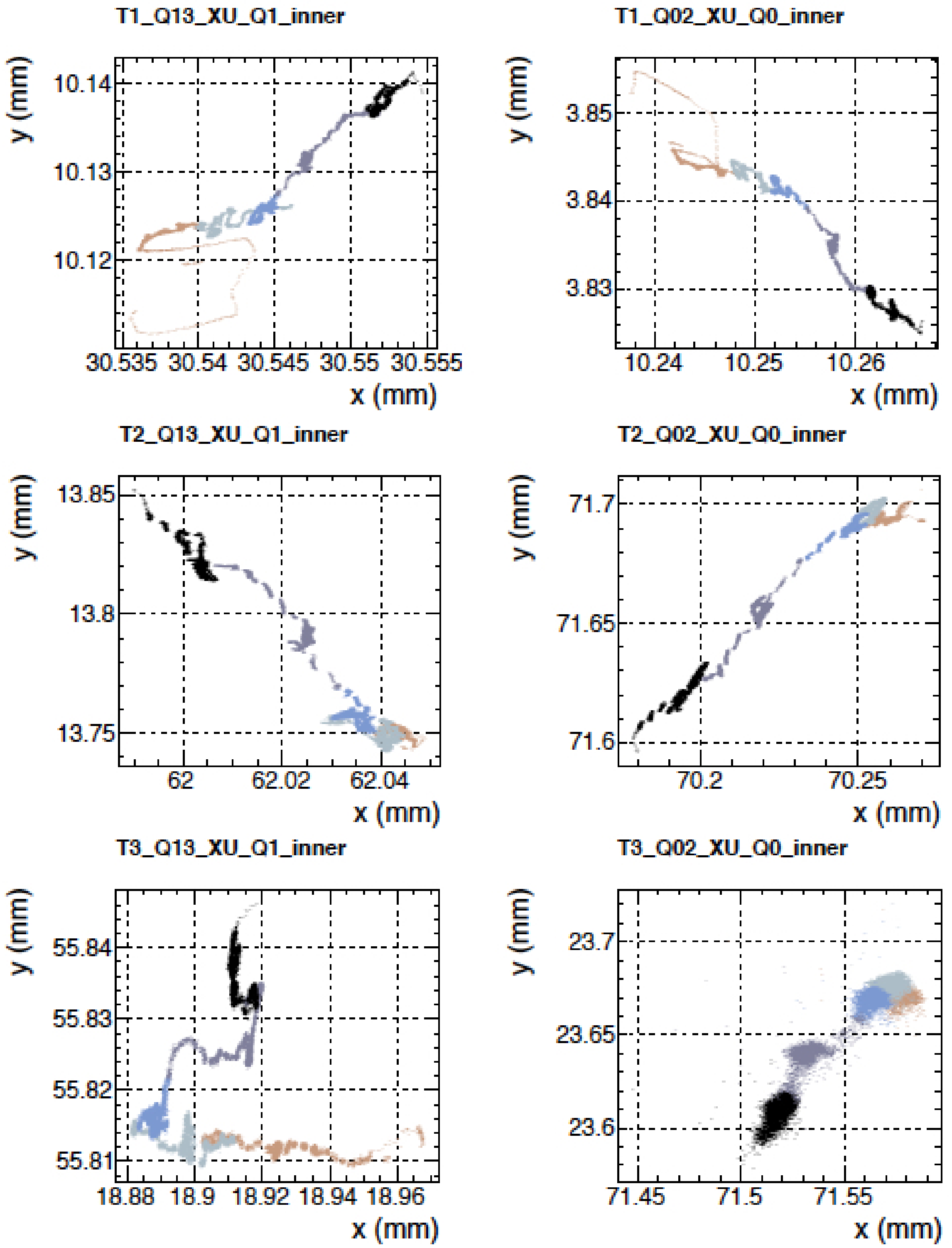

Figure 25: The movement of internal bottom corners of **XU C-frames** in x, y plane in a period of 22 September – 10 October 2016 for T1-T3 stations. The data are divided into five equal periods subsamples from light brown color to dark blue and black, from the first to the last subsample of time, respectively.

3.2 Measurements of C-frame lengths

A temperature is one of the environmental conditions which can cause changes in the lengths of C-frames. But in the analyzed period, the temperature inside the detector was rather stable and close to 19.6^0 C (Fig. 26). Only from the end of May until the beginning of June the temperature was lower by roughly 0.5^0 C. For the temperature changes by half degree the decrease of the length for 3m long aluminium rod is expected to be 35 μm.

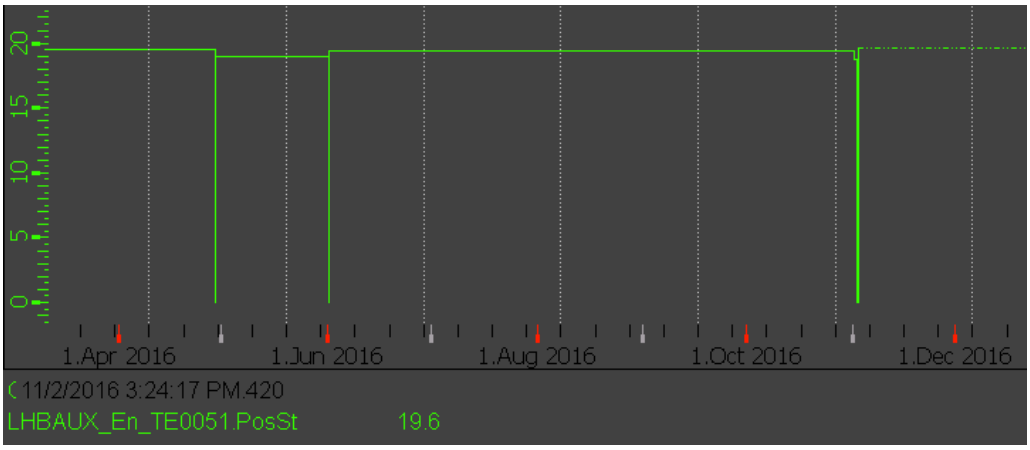

Figure 26: The temperature in 2016 from April till December measured inside the LHCb detector. The three vertical lines correspond to breaks in the measurements caused by the power cuts.

Other reasons of the length modifications for C-frames could be material stresses caused by opening and closing the detector or effects of switching the magnet.

Lengths can be calculated from the measured x and y coordinates of points close to the corners of each OT frame according to the equation:

$$R = \sqrt{(x_1 - x_2)^2 + (y_1 - y_2)^2} \tag{1}$$

The indexes 1 and 2 in the above equation correspond to two points measured by RASNIK, between which the distance is calculated. All calculated lengths are defined in Fig. 27. Since results from the lines mounted on the external bottom corners of C-frames are not available, only the seven distances L0, L1-L6 are defined for each plane of the OT stations. The L0, L1 and L4 are calculated between points which are close to the top of C-frames. The L2, L3, L5 and L6 lengths are calculated using the points which are close to the internal bottom corners of C-frames.

The measured length changes are presented in Figs 28-33 for all C-frames. The L0 length is approximately a sum of L1 and L4. These lengths are stable in time of more than seven months. The observed changes are within a few μm. The variations up to 200 μm are observed for L2, L3, L5 and L6. For these lengths, the largest modifications are observed in May 2016. From July till September, the lengths are rather stable. In October and November, the changes are opposite to the ones observed in May. These changes cannot

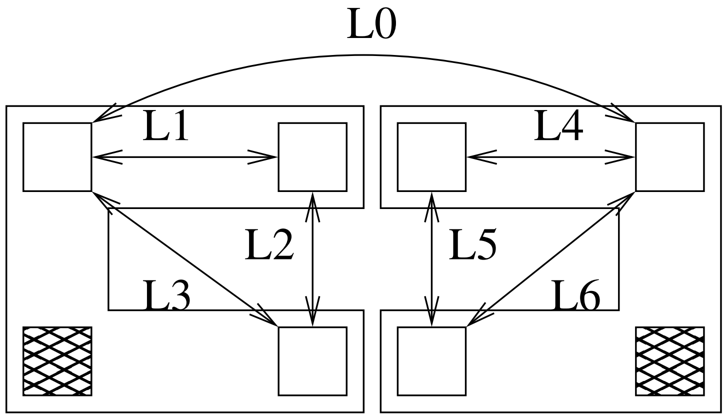

Figure 27: Definitions of lengths L0-L6 between the points measured by RASNIK lines which are symbolically marked by the squares. The lines are placed in the same way as they are mounted on C-frames for VX and XU planes of each OT station. The hatched squares indicate the lines which are not working. The drawing is only schematic and does not preserve the scales.

be explained by the temperature variations and are related with mechanical stresses. They are reflections of distortions observed in correlation distributions in Figs 22-25.

To conclude, the length variations of C-frames due to the temperature change are negligible. The observed length changes, of the order of 200 μm, are caused by the mechanical stresses.

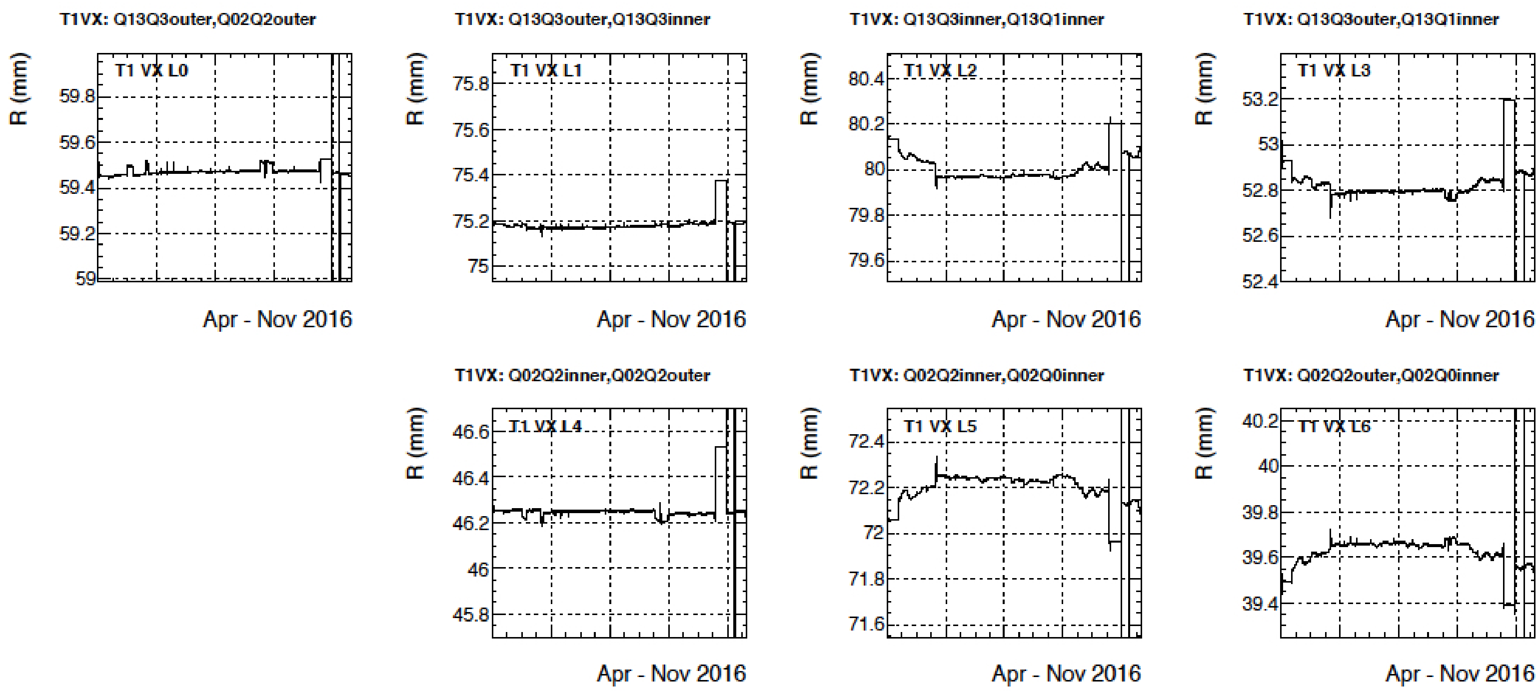

Figure 28: The length (R) distributions for L0–L6 lengths in time for the data acquired in 2016 for **VX C-frames of T1 station**.

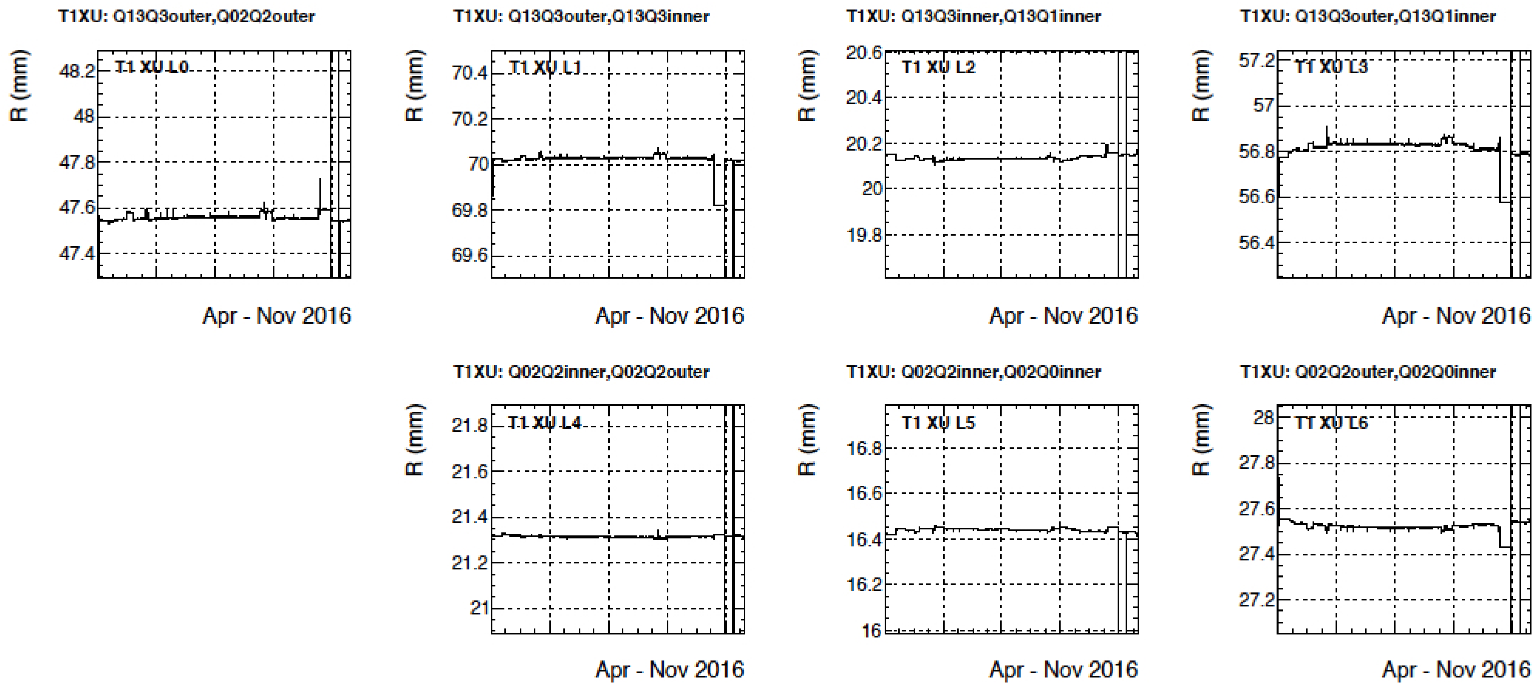

Figure 29: The length (R) distributions for L0–L6 lengths in time for the data acquired in 2016 for **XU C-frames of T1 station**.

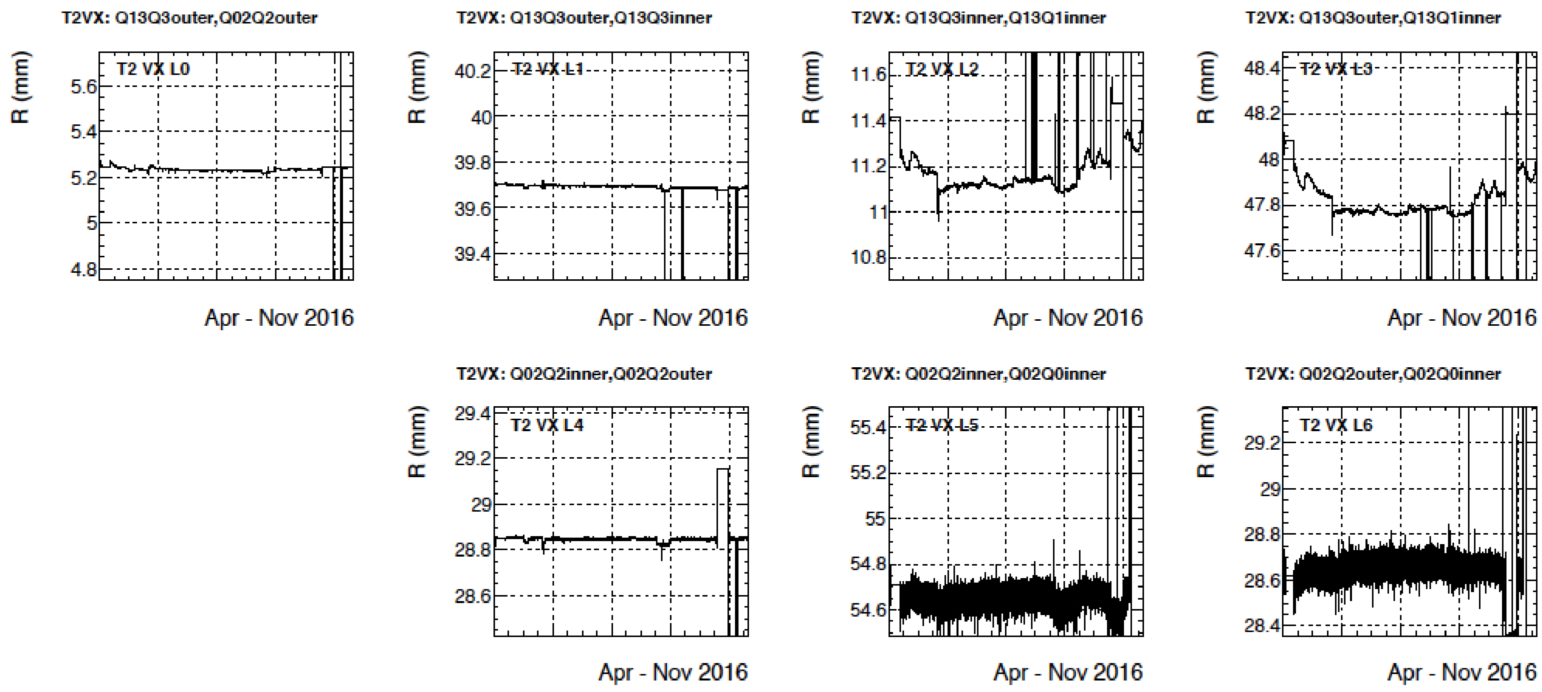

Figure 30: The length (R) distributions for L0–L6 lengths in time for the data acquired in 2016 for **VX C-frames of T2 station**.

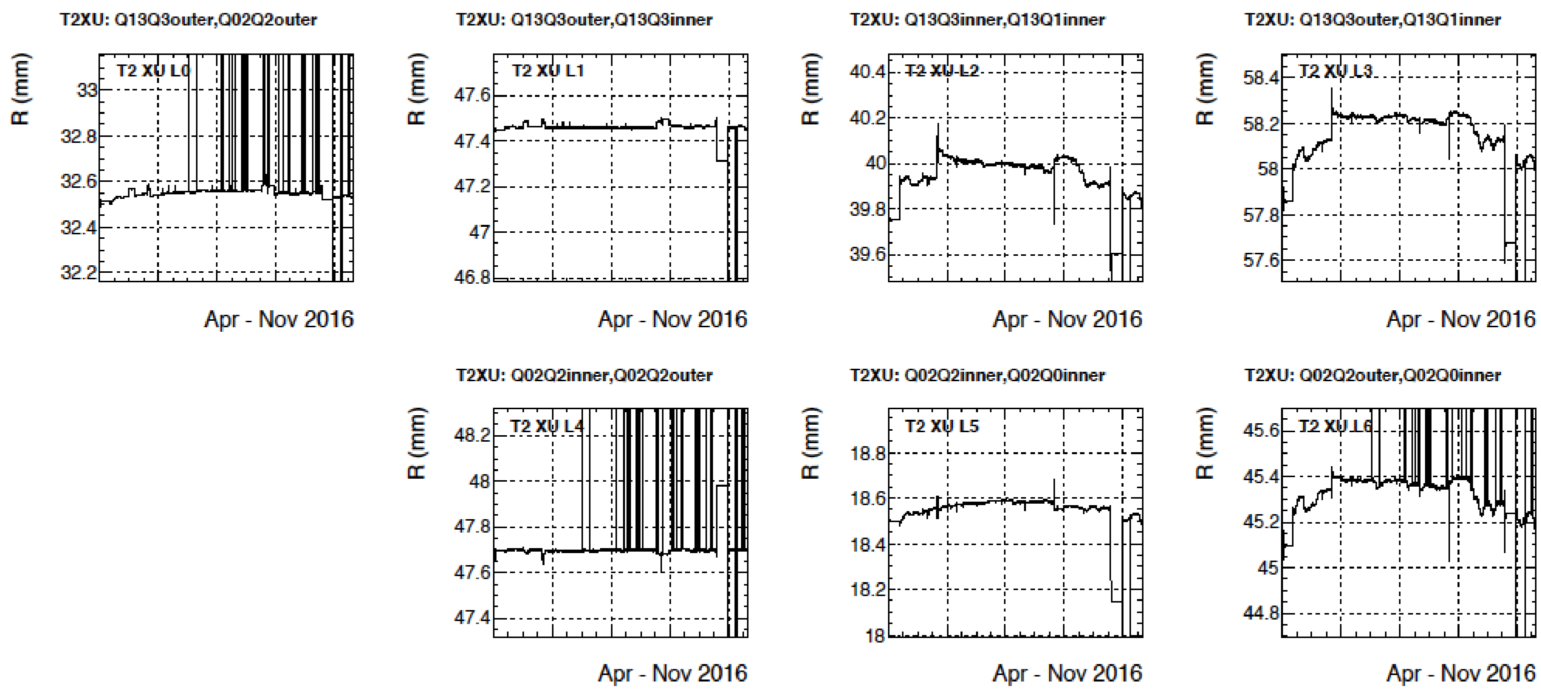

Figure 31: The length (R) distributions for L0–L6 lengths in time for the data acquired in 2016 for **XU C-frames of T2 station**.

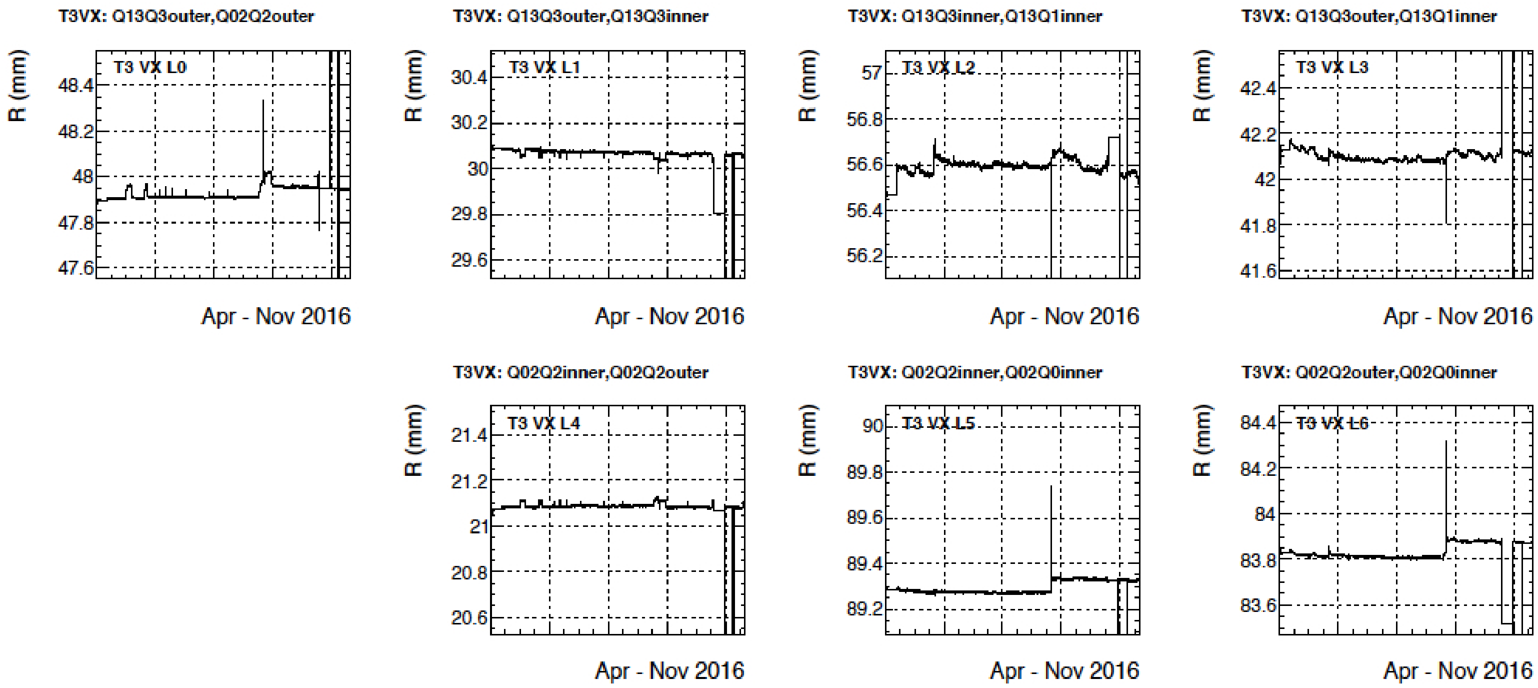

Figure 32: The length (R) distributions for L0–L6 lengths in time for the data acquired in 2016 for **VX C-frames of T3 station**.

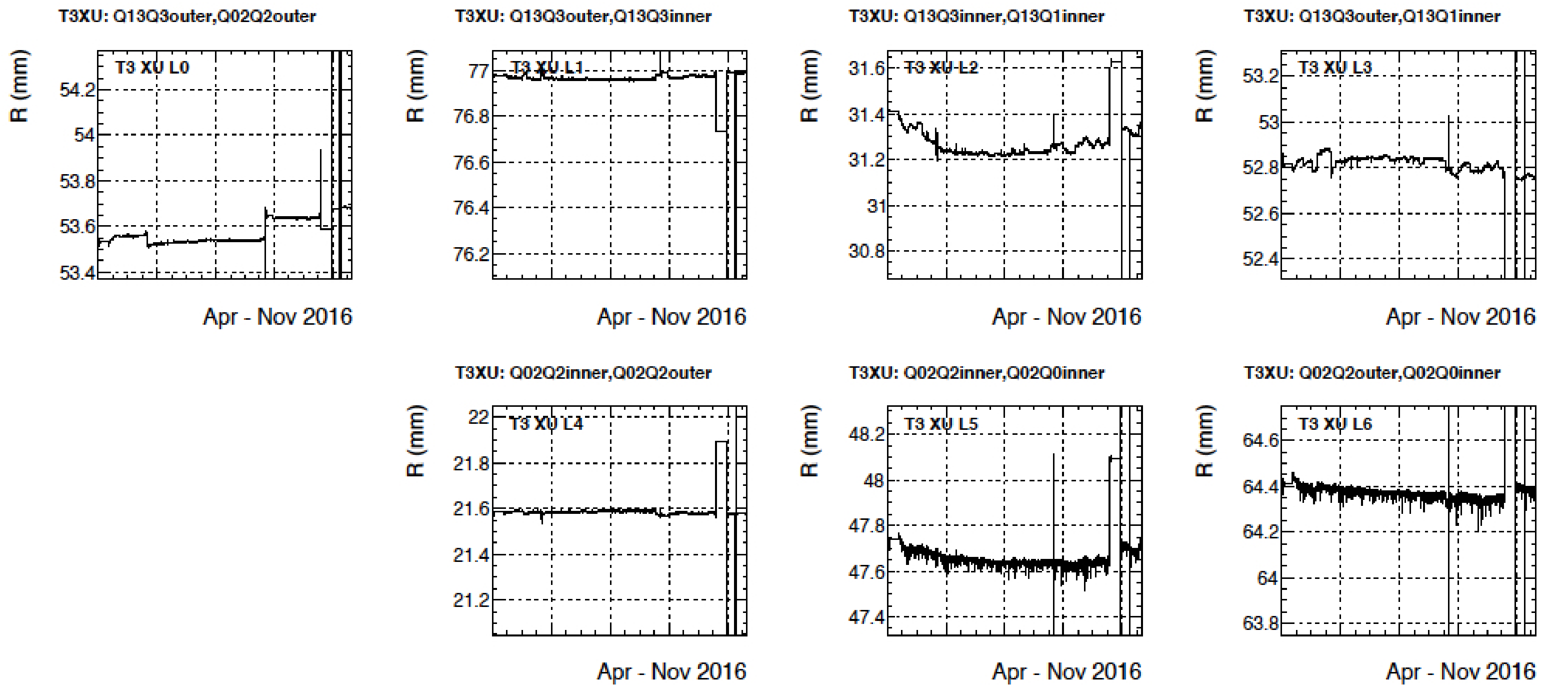

Figure 33: The length (R) distributions for L0–L6 lengths in time for the data acquired in 2016 for **XU C-frames of T3 station**.

3.3 Effects of opening and closing C-frames

The two C-frames VX and XU of T3 station on the C-side were opened and closed on 15$^{\text{th}}$ September 2016. To check how this intervention affects the positions in the OT, the data from one day before and one day after that event are presented. The measured x and y values in this period are shown in Figs 34 and 35 for VX and XU planes, respectively. The opening and closing of C-frames produces small shifts in both the x and y values. The horizontal shift of about 70 μm in the x is significantly larger than about 20 μm in the vertical y.

The intervention in T3 station on C-side can also affect C-frames of T1 and T2 stations since the opening of a frame can result in small changes of the bridge position. The observed variations are significantly smaller than in the opened station. As an example, the measured modifications for T2 station VX plane for both A-side and C-side are presented in Figs 36 and 37, respectively. The x and y values measured in the periods before and after intervention are similar and the changes in magnitudes are not larger than 20 μm.

The RASNIK measurements show that the positions of C-frames are reproducible after opening and closing within $\pm$70 μm.

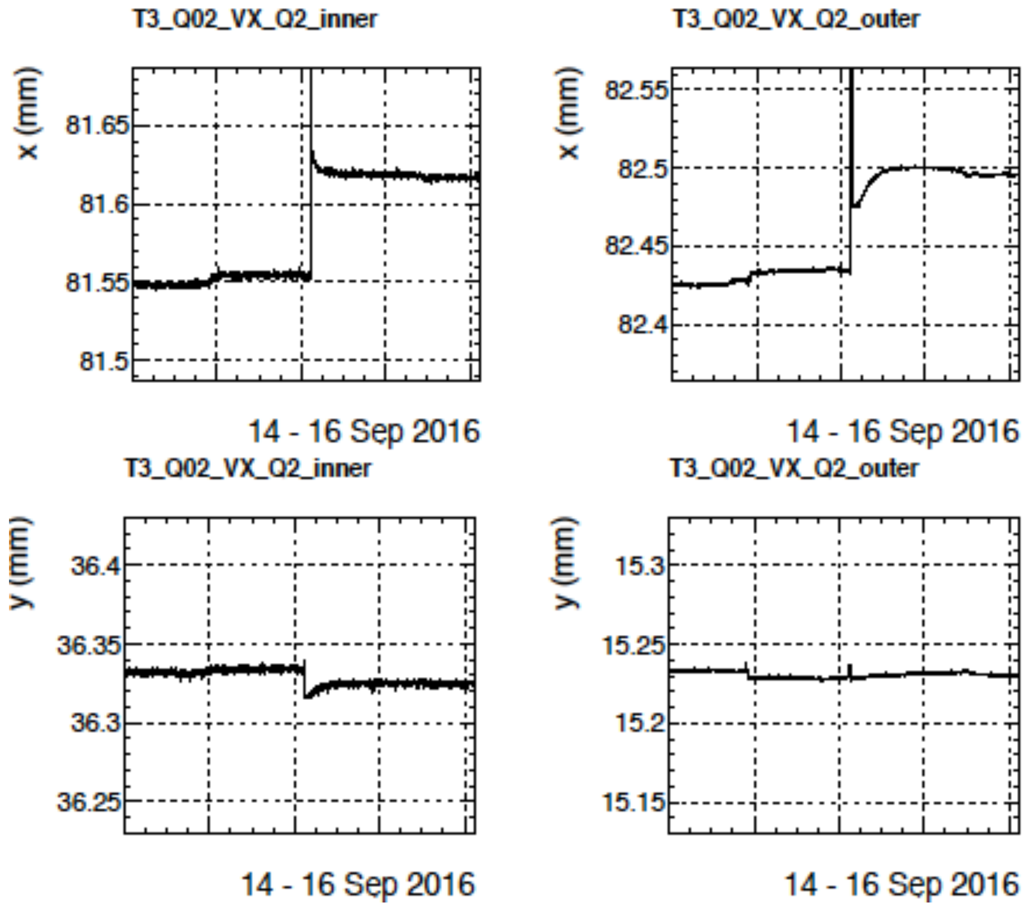

Figure 34: The x and y coordinates of points close to the top corners of opened and closed **VX C-frame** as a function of time (14-16 of September 2016) measured for **T3 station** on the C-side.

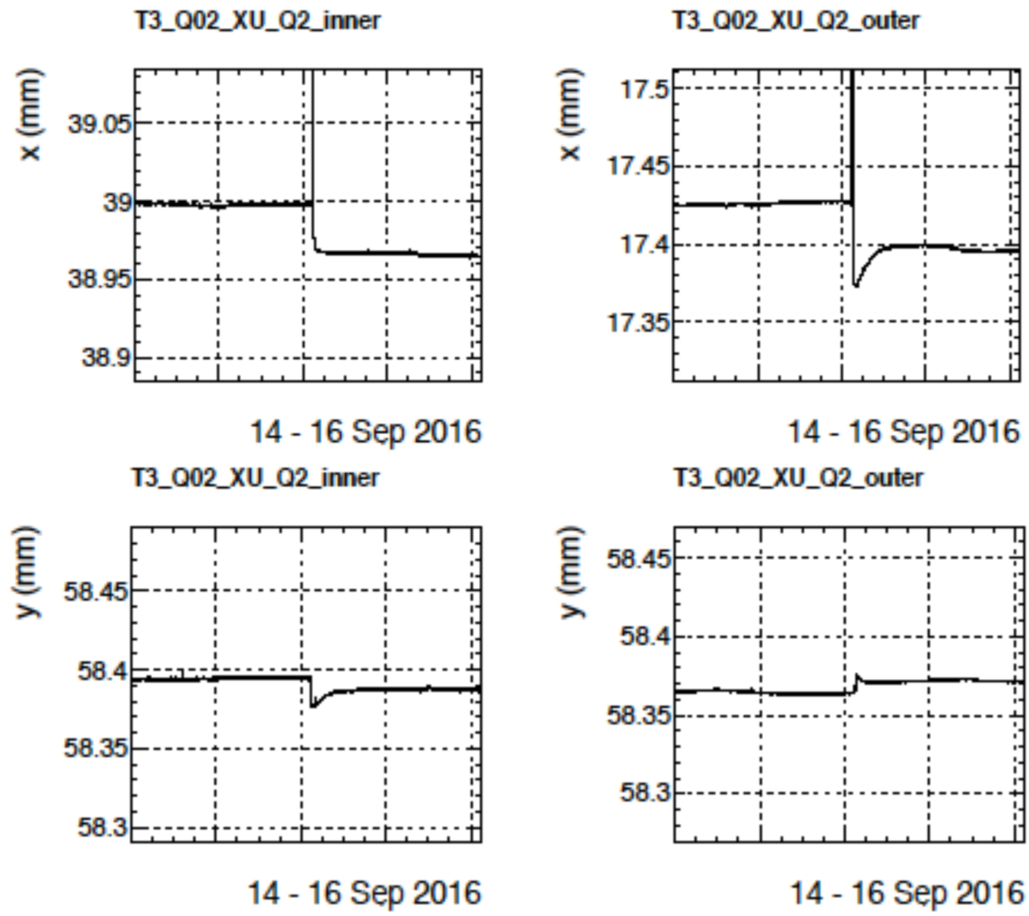

Figure 35: The x and y coordinates of points close to the top corners of opened and closed **XU C-frame** as a function of time (14-16 September 2016) measured for **T3 station** on the C-side.

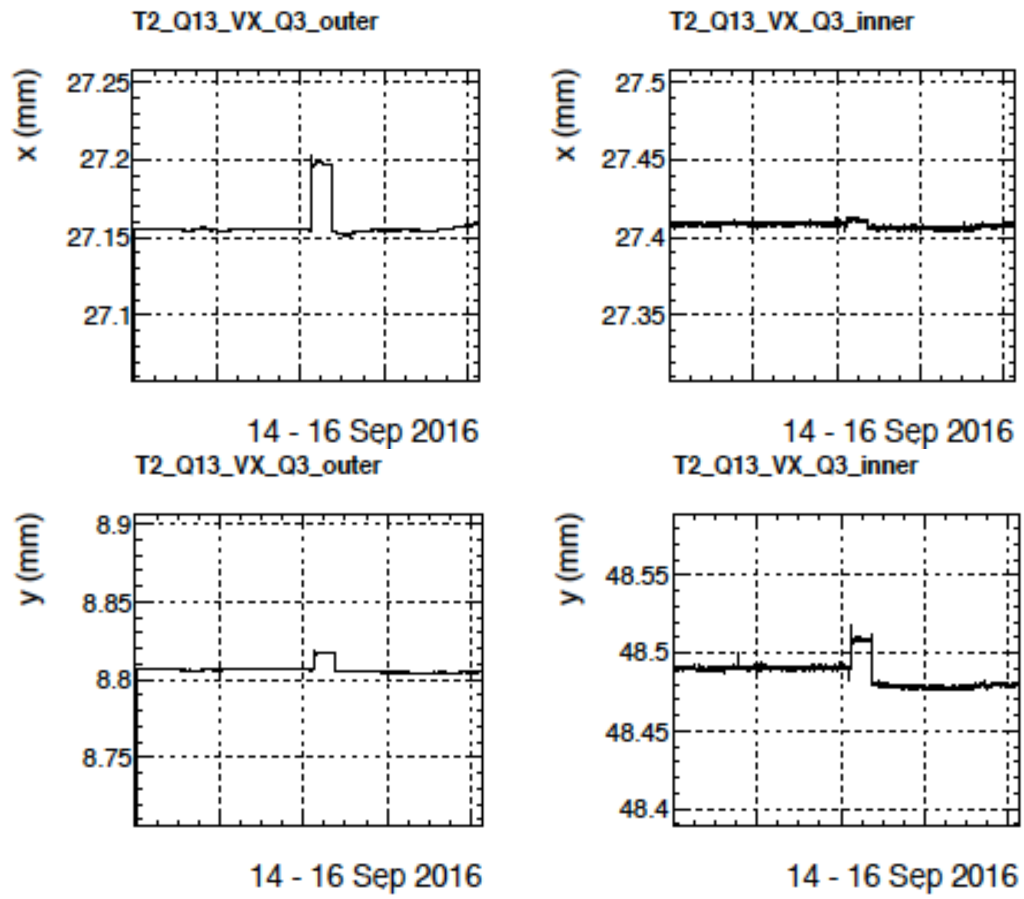

Figure 36: The x and y coordinates of points close to the top corners of **VX C-frame** as a function of time (14-16 September 2016) measured for **T2 station on the A-side**.

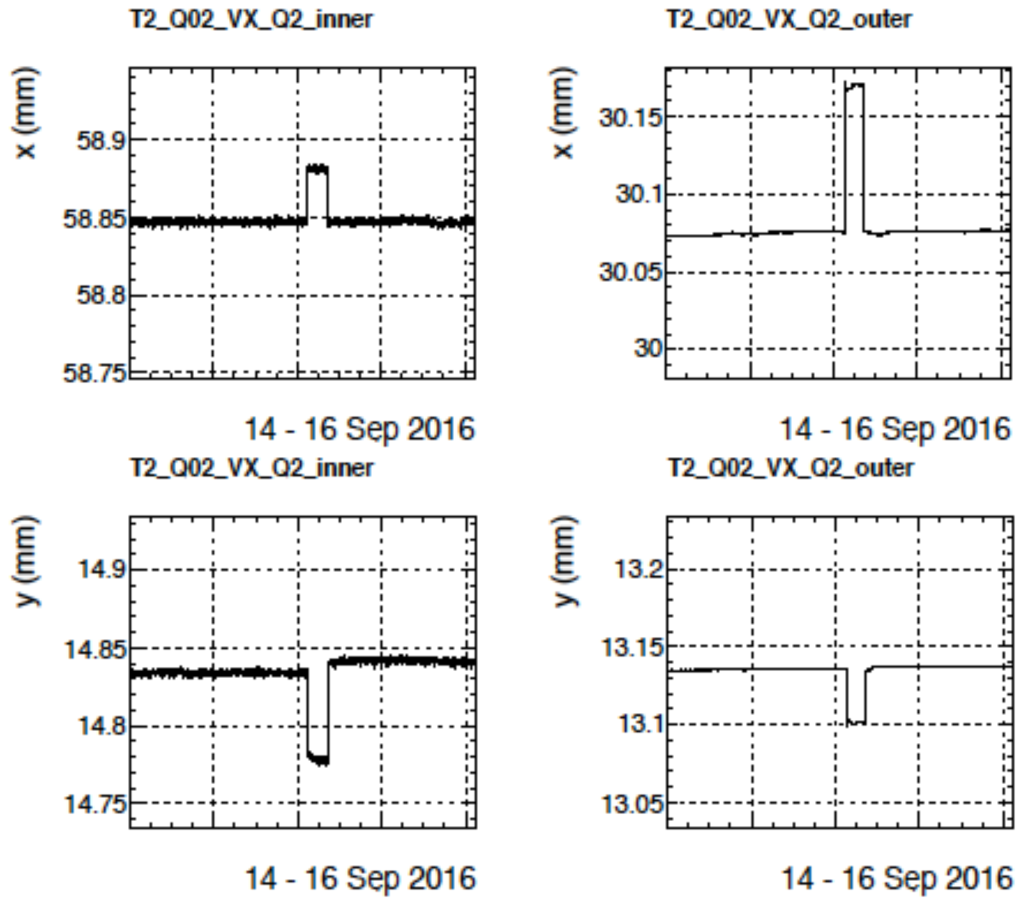

Figure 37: The x and y coordinates of points close to the top corners of **VX C-frame** as a function of time (14-16 September 2016) measured for **T2 station on the C-side**.

4 Monitoring of the bridge position by two vertical RASNIK lines

The Q02 and Q13 lines allow to study the movements of the bridge with respect to the bunker. These lines measure the x and z LHCb coordinates of the points close to the top and on the opposite sides of the bridge (Fig. 8).

4.1 Long term stability of the bridge position – the "z and x effect"

The x and the z values measured using Q02 and Q13 lines in 2016, as well as their correlations, are shown in Fig. 38. The variations in the x are smaller than in the z by about a factor of two. In May and June 2016, the z decreases by about 100 μm and stabilizes in August/September. There is a hint that a trend reverses at the end of the year and the z starts to increase. Correlations between the z and x are observed. This effect is the largest in May and June, where there are the largest movements in the z. The RASNIK system shows that the effect is caused by the movement of the OT bridge with respect to the bunker. The measurements only in May and June in the x and z coordinates are presented in Fig. 39. The "jumps" which are seen in the x and z distributions are related with power cuts or switching on/off of the magnet.

The shifts in the z coordinate of the bridge position observed by the RASNIK system are also seen in similar way by the Software Alignment Group [6] and the BCAM (Brandeis CCD Angle Monitor) opto-electronic position system which monitor the movements of the IT stations [7].

In summary, the movements of the bridge with respect to the bunker are observed. The positions stabilize in August and September. At the end of 2016, the bridge tends to move in the opposite direction. The largest changes are observed in the z coordinate, but movement in x coordinate is also observed.

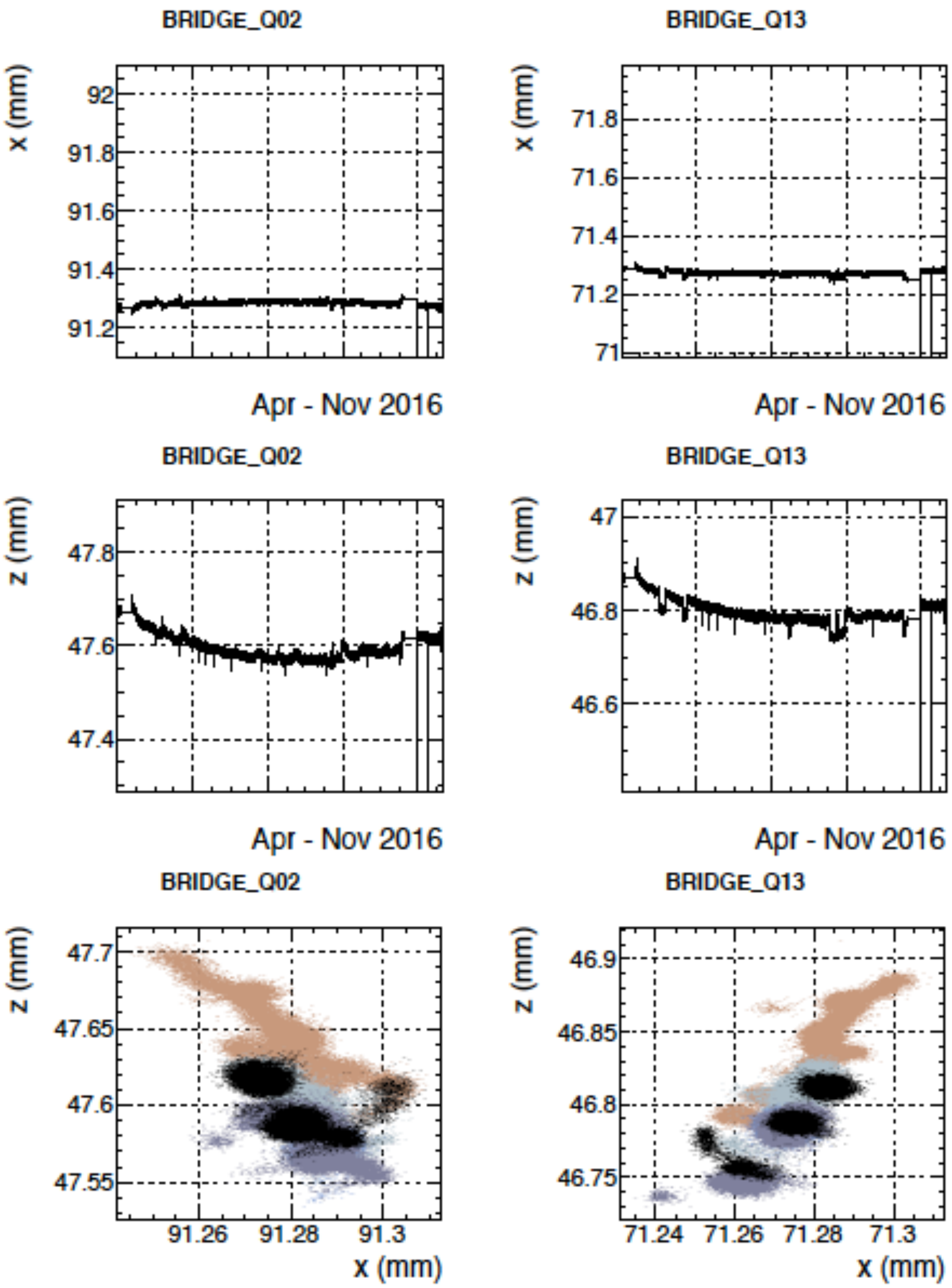

Figure 38: The x (top) and the z (middle) bridge position coordinates distributions in time and their correlations (bottom). To show time dependence of the z vs x correlations in time, the data are divided into five subsamples, of equal periods, from light brown color to dark blue and black, from the first to the last periods of time, respectively.

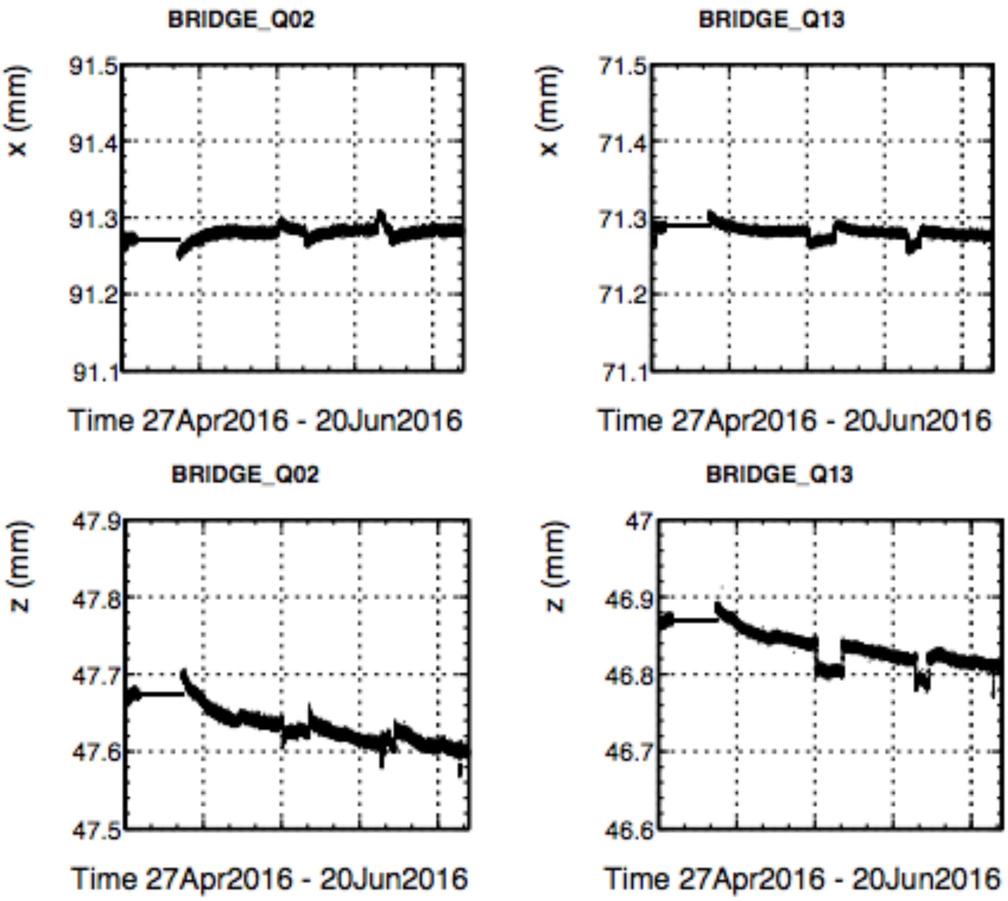

Figure 39: The x (top) and the z (bottom) distributions coordinates in time, corresponding to a period from 27 April till 20 June. The results are obtained using the two lines Q02 and Q13 which measure the movements of two top points on the opposite sides of the bridge with respect to the bunker. The visible two "jumps" are connected with switching off of the magnet on 23-26 of May and on 6-9 of June in 2016.

4.2 Movements of the Outer Tracker supporting bridge in the magnetic field

To study the dependence of observed shifts in the z coordinate on the direction of the magnetic field, the periods with two downstream and one upstream polarization are:

- 6-21 May 2016 (downstream polarization),
- 26 May - 6 June 2016 (downstream polarization),
- 9-18 June 2016 (upstream polarization).

Movements of the bridge in the z and x plane in each period are presented in Fig. 40. To study the details of the movements, in each sample the data are divided into five equal period subsamples. The bridge moves both in the z and the x direction in each term, while the largest modifications are observed in the first period (6-21 May 2016). The changes in the x are smaller than in the z by about a factor of two. After relatively fast initial movements of the bridge in each period it reaches the equilibrium position.

To study the influence of the change in magnitude of the magnetic field on the position of the OT, the data from the period from 21 of May until 10 of June 2016 are chosen. The magnet was switched off twice, on 23-26 of May and on 6-9 of June. Before 23 of May, as well as between 26 of May and 6 of June, the polarization of the magnet was down. After 9 of June, the polarization was up. To study the movements due to a change of the magnetic field the four periods of time were chosen:

- 21-24 May 2016 (change from down polarization to switching off),
- 25-27 May 2016 (change from switching off to down polarization),
- 5-7 June 2016 (change from down polarization to switching off),
- 8-10 June 2016 (change from switching off to up polarization).

The shifts of the bridge with respect to the bunker in the z and x coordinate planes, measured using Q02 and Q13 lines, are shown in Figs 41 and 42, respectively. In each period, the data are divided into five subsamples corresponding to different colors, from light brown to dark blue and black, from the first to the last subperiods. It allows to study variations of the x and z in time. The x and z values are similar before and after switching off of the magnet. The dependence of the bridge position on different types of polarization of the magnet is not observed, as shown in Figs 41 and 42. Only switching off of the magnet gives significant modifications in the x and z. In the analyzed periods, the movements are larger for Q13 line (Fig. 42) than for Q02 line (Fig. 41). One side of the bridge shifts more than the opposite side with respect to the bunker after switching on the magnet.

To summarize, the switching off of the magnet causes the movement of the bridge, but after switching on the magnet again the bridge moves back to the previous position. The dependence of the bridge position on down and up types of polarization of the magnet is not observed.

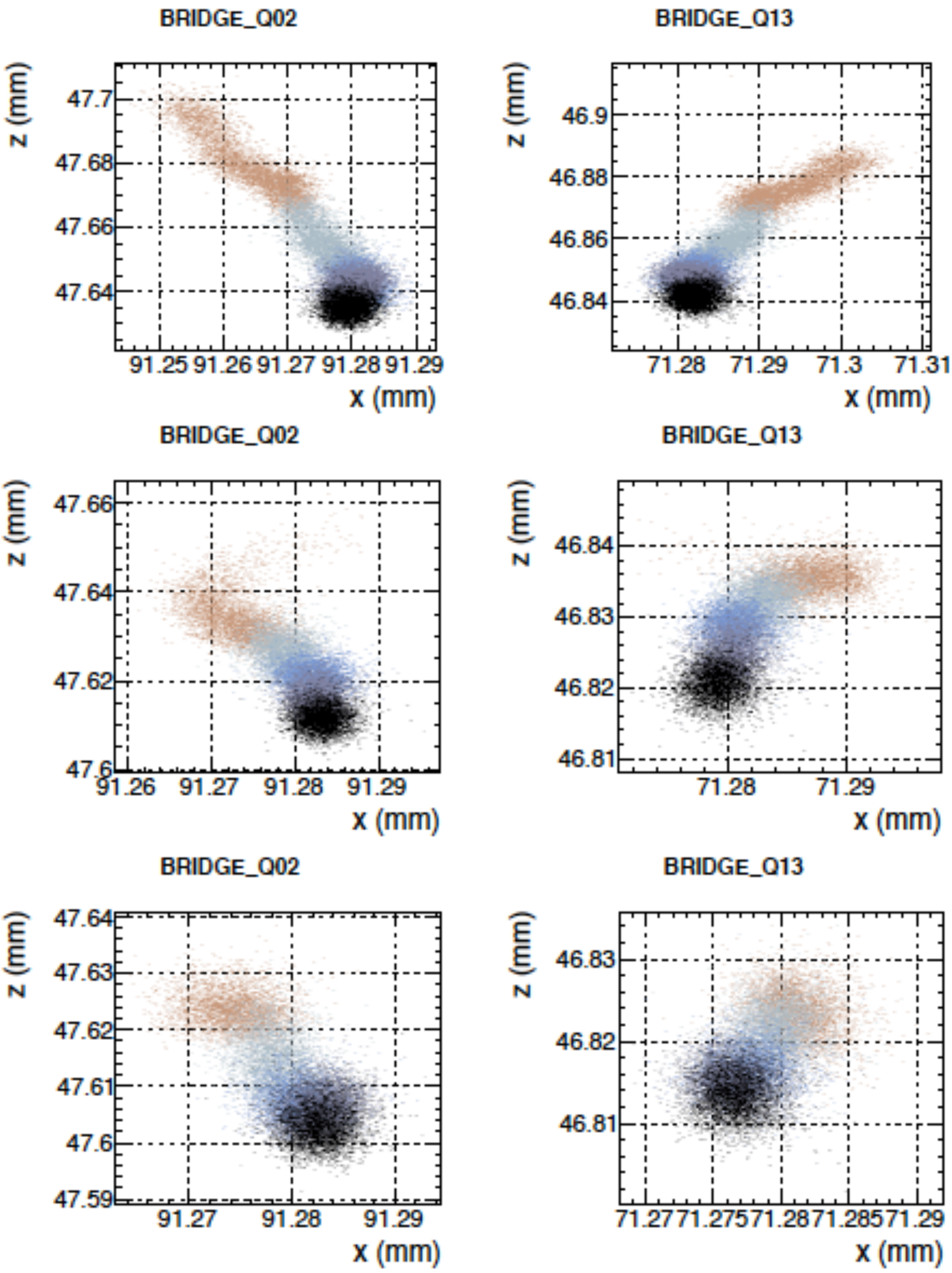

Figure 40: The z vs x correlations in three periods of data taking corresponding to a given polarization of the magnet: top – downstream polarization (6-21 May 2016), middle – downstream polarization (26 May - 6 June 2016) and bottom – upstream polarization (9-18 June 2016). The results are obtained using the two RASNIK lines, Q02 (left column) and Q13 (right column), which measure movements of the bridge with respect to the bunker. In each period the data are divided into five equal period subsamples from light brown color to dark blue and black, from the first to the last subsample of time, respectively.

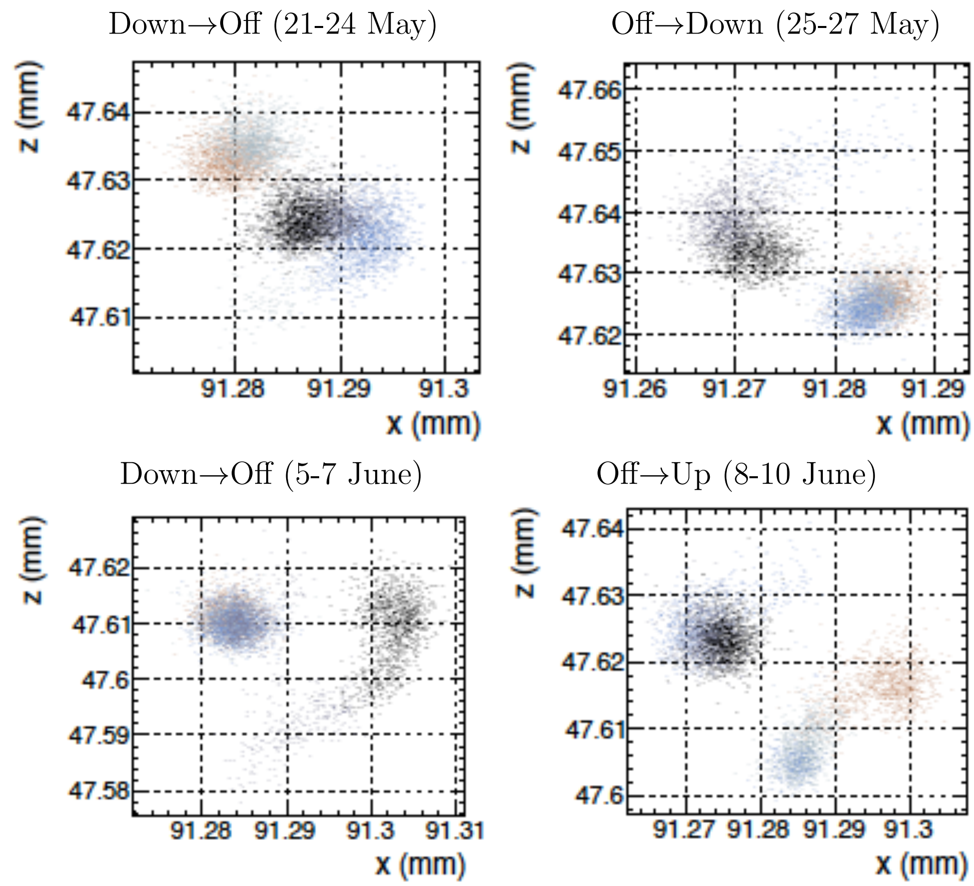

Figure 41: The z vs x correlations in the selected four periods, in which the status of the magnet was changed as follows: from down polarization to switching off (21-24 May 2016), from switching off to down polarization (25-27 May 2016), from down polarization to switching off (5-7 June 2016) and from switching off to up polarization (8-10 June 2016). The results are obtained using **Q02 line** which measures the movements of the top point of the bridge with respect to the bunker. In each period the data are divided into five equal time subsamples from light brown color to dark blue and black, corresponding to the first and to the last subsamples of time, respectively.

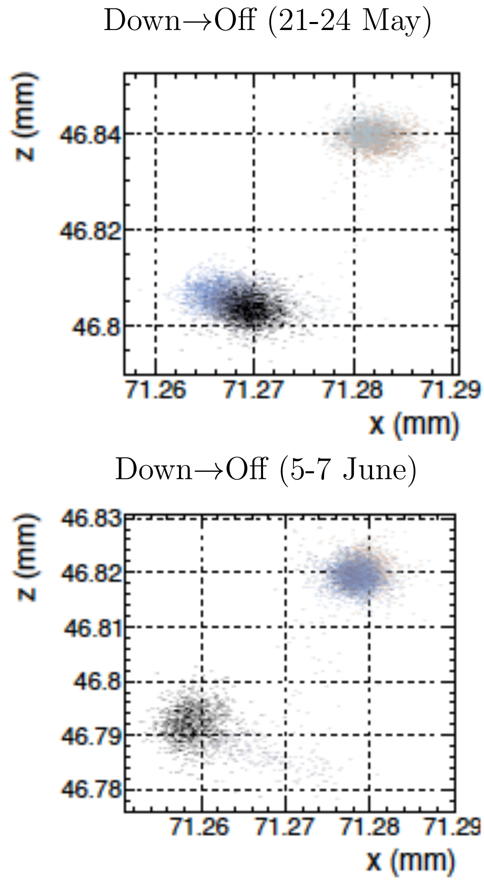

Figure 42: The z vs x correlations in the selected four periods in which the status of the magnet was changed as follows: from down polarization to switching off (21-24 May 2016), from switching off to down polarization (25-27 May 2016), from down polarization to switching off (5-7 June 2016) and from switching off to up polarization (8-10 June 2016). The results are obtained using **Q13 line** which measures the movements of the top point of the bridge with respect to the bunker. In each period the data are divided into five equal time subsamples from light brown color to dark blue and black, corresponding to the first and to the last subsamples of time, respectively.

4.3 Variations for the bridge position due to opening and closing C-frames

The two C-frames VX and XU of T3 station on C-side were opened and closed on 15$^{\text{th}}$ September 2016 (see Sec. 3.3). This intervention affects also position of the bridge with respect to the bunker. Results are shown in Fig. 43. The x and z positions are similar before and after opening and closing the C-side frames of T3 station, showing slightly larger deviations only in the opened stage of the detector.

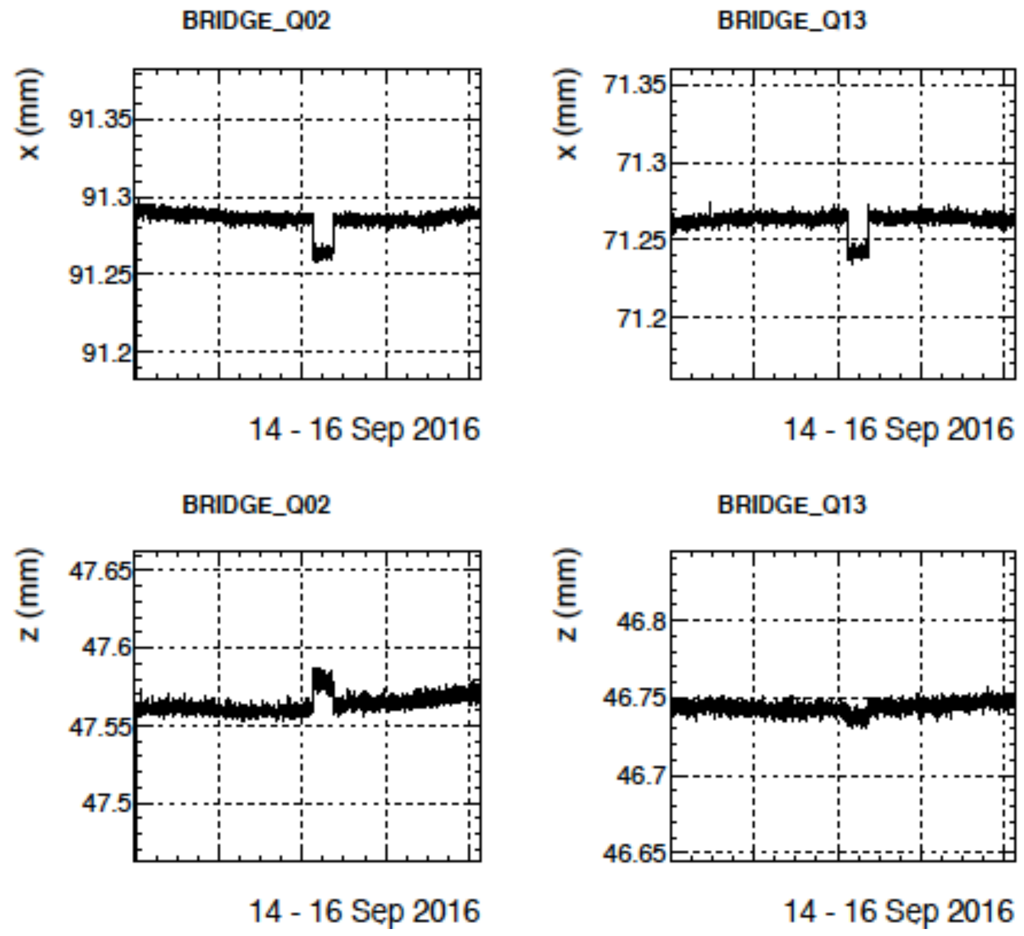

Figure 43: The x and z coordinates in a function of time (14-16 September 2016) measured by the two lines: Q02 (left column) and Q13 (right column) which monitor movements of the bridge with respect to the bunker.

5 Conclusions

The RASNIK system has been built to monitor the positions in the Outer Tracker detector. It has been operating in the all running periods of LHC. In this paper we have analyzed the data taken in 2016. They consist of a part of Run 2 of LHC.

The results show that to a very good approximation the construction supporting the Outer Tracker detector is mechanically a rigid system. High accuracy of the RASNIK data allow, however, to track even small deformations of the Outer Tracker detector connected with magnetic field configurations, mechanical interventions etc. The RASNIK lines can also support software alignment with the precision data showing the real movements of the detector. It is a robust system for position control of the Outer Tracker stations.

References

[1] LHCb collaboration, A. A. Alves Jr. *et al.*, *The LHCb detector at the LHC*, JINST **3** (2008) S08005.

[2] H. Dekker *et al.*, *The RASNIK/CCD 3-Dimensional Alignment System*, eConf **C930928** (1993) 017.

[3] H. Van Der Graaf *et al.*, *RASNIK, the Alignment System for the ATLAS MDT Barrel Muon Chambers*, Technical System Description, Amsterdam 2000.

[4] M. Adamus *et al.*, *Test results of the RASNIK optical alignment monitoring system for the LHCb Outer Tracker Detector*, LHCb-Note-2001-004.

[5] M. Adamus *et al.*, *First Results from a Prototype of the RASNIK Alignment System for the Outer Tracker Detector in LHCb Experiment*, LHCb-Note-2002-016.

[6] M. Martinelli, *Outer Tracker Alignment in 2016*, Presentation during LHCb Week, 20 June 2016.

[7] P. Stefko, *Online Inner Tracker position monitoring*, PhD Thesis in preparation, Laboratoire de Physique des Haites Energies.